Detector Technology

Performance optimization of detector electronics for millimeter laser ranging

S. Cova[+], *A. Lacaita*[+] *and G. Ripamonti**

[+]Politecnico di Milano, Dipartimento di Elettronica e Informazione and CEQSE-CNR,
Piazza L. da Vinci 32 - 20133 Milano (Italy)

*Universita' degli Studi di Milano, Dipartimento di Fisica
Via Celoria 16 - 20133 Milano (Italy)

(invited paper)

ABSTRACT

The front-end electronic circuitry plays a fundamental role in determining the performance actually obtained from ultrafast and highly sensitive photodetectors. We deal here with electronic problems met working with Microchannel Plate photomultipliers (MCP-PMTs) and Single Photon Avalanche Diodes (SPADs) for detecting single optical photons and measuring their arrival time with picosecond resolution. The performance of available fast circuits is critically analyzed. Criteria for selecting the most suitable electronics are derived and solutions for exploiting at best the detector performance are presented and discussed

I. INTRODUCTION

Laser ranging applications with millimeter resolution require to measure the time of flight of single photons with precision better than 30ps root mean square (rms), that is, with better than 70ps full-width at half maximum (FWHM) of the resolution curve. Two photodetector types can attain single photon sensitivity and picosecond resolution: proximity-focused Microchannel Plates (MCPs) [1-3] and Single Photon Avalanche Diodes (SPADs) [4-7]. In both cases the front-end electronics associated to the detector plays a fundamental role. In order to take full advantage of the detector timing performance, the electronic pulse processing should be carefully optimized.

In set ups where MCPs are employed, the fast preamplifier and the constant fraction trigger circuit (CFT) are by far the most critical electronic components. In this paper we discuss criteria for optimum selection of the preamplifier, taking into account the noise and bandwidth characteristics. We show that preamplifiers with very large bandwidth (3GHz or more) are not to be employed, since they impair the timing performance [8]. We analyze problems met by constant fraction triggers working with

subnanosecond pulses from MCPs. We discuss how the performance of available CFTs can be improved by simple modifications that provide a better adjustment of the relevant CFT parameters and/or by suitable pre-filtering of the MCP pulses [9,10].

SPADs are avalanche photodiodes that operate biased above the breakdown voltage in the so-called Geiger-mode [4-7,11]. Their operation is fundamentally different from that of photomultiplier tubes (PMTs) and of ordinary avalanche photodiodes (APDs). The device does not have a linear internal gain, that is, it does not amplify linearly the primary photocurrent. It instead exploits the avalanche process to behave in a way similar to that of a trigger circuit, rather than an amplifier. When one or more photons are detected at a given time, a fast-rising current pulse is generated, with standard amplitude and shape, independent of the number of photons. The leading edge of this pulse marks with very high precision, down to 20ps FWHM, the time of arrival of the photon that has triggered the avalanche [5].

We analyze limitations met working with SPADs in the simple biasing arrangements that employ a ballast resistor to quench the avalanche, called Passive Quenching Circuits (PQCs) [6,7,11]. In order to fully exploit the ultimate SPAD timing performance, the device should be operated with an Active Quenching Circuit (AQC) [12,13]. We introduce a new AQC model, capable of driving the detector in remote position, connected by a coaxial cable [13]. Special care has been devoted to the design of the input stage, in order to minimize the circuit noise and thus reduce to less than 3ps rms the internal time jitter of the circuit, making negligible its contribution to the overall time resolution.

II. SELECTION OF THE OPTIMUM PREAMPLIFIER FOR MCPs

Since the gain of the MCP is limited to 5 10^5, a fast preamplifier with gain higher than 10 must be used between the MCP output and the pulse-timing trigger circuit. This gain makes the noise of the following circuits negligible, in comparison to that of the amplifier. In order to avoid reflections and ringing in the pulse shape, the MCP output must be terminated on a 50 Ohm resistor R_s , as outlined in the equivalent circuit of Fig.1.

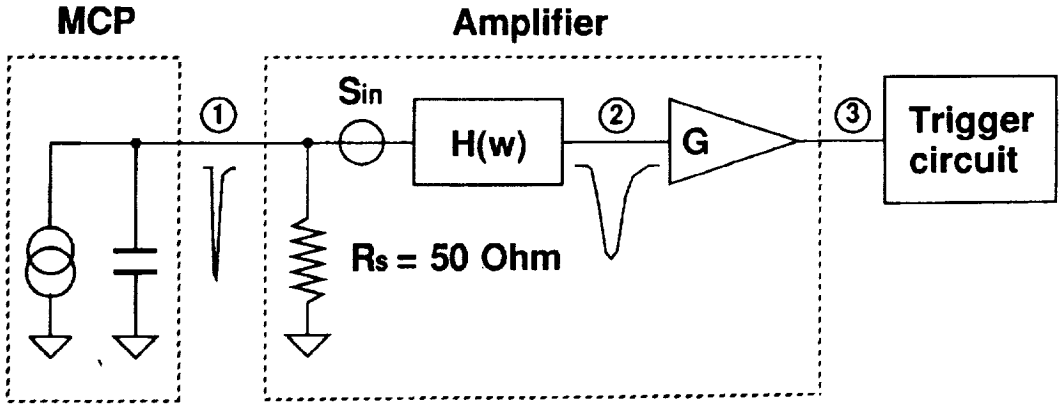

Fig.1 Equivalent circuit for analyzing the effect of the amplifier noise and bandwidth on the pulse time-jitter.

An accurate analysis of the time-jitter contribution arising from the electronic noise has been carried out [8] and we report here the main results. The action of the amplifier on the MCP pulses is described (see Fig.1) by two blocks: a transfer function in the frequency f domain $H_A(f)$, normalized to unity dc gain, followed by a constant gain G. The time-domain impulse response of the amplifier is $h_A(t) = F^{-1}[H_A(f)]$ (where F^{-1} denotes the inverse Fourier transform and $h_A(t)$ is normalized to unit area). S_i is the spectral density of the equivalent input noise generator of the amplifier, assumed to be gaussian. As sketched in Fig.2, the noise causes a random shift of the actual crossing time of the trigger threshold.

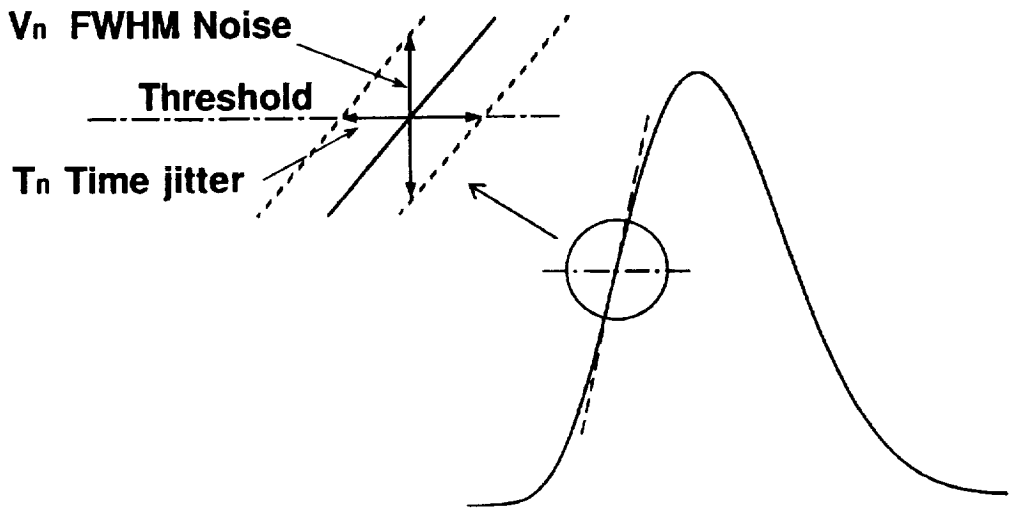

Fig.2 Effect of the electronic noise on the triggering time.

Let us denote by v_n the rms value and by V_n the FWHM of the amplitude distribution of the noise, and by r the slope of the ideal, noise-free pulse at the triggering threshold. The FWHM T_n of the additional time jitter is given by

$$T_n = \frac{V_n}{r} = 2.36\frac{v_n}{r} \qquad (1)$$

This time jitter at the comparator threshold (point 3 in Fig.1) is equivalently evaluated at the input of the gain stage G (point 2 in Fig.1).

In first instance, the noise spectrum can be considered white, that is, with constant spectral amplitude $S_i = a^2$. Let us denote by B_n the noise bandwidth, proportional to the signal bandwidth B_A (3dB down bandwidth)

$$B_n = K_n B_A \qquad (2)$$

with constant K_n depending on the shape of the frequency response $H_A(f)$. We have

$$v_n = a\sqrt{B_n} = a\sqrt{K_n B_A} \qquad (3)$$

The slope r also increases with B_A , and it can be easily seen that there is a minimum in the plot of T_n versus B_A. Let us first consider the high bandwidth side, where the B_A values are high enough to have risetime practically equal to that of the MCP pulse. On that side, T_n goes up as $\sqrt{B_A}$, since the slope r is unaffected and the noise v_n increases as $\sqrt{B_A}$. Let us now consider the low bandwidth side, where the pulse-risetime T_r is fully dominated by B_A, namely, T_r is about $1/(3\ B_A)$. On this side, T_n goes down as $B_A^{-3/2}$ when B_A is increased, since the slope r increases as B_A^2 and noise increases as $\sqrt{B_A}$. A minimum of T_n will therefore be found at an intermediate value of B_A , at which the relative rate of increase of the pulse slope r will be equal to that of the noise V_n. More accurate quantitative results can be obtained by considering the actual voltage waveform. Let us denote by $V_D(t)$ the voltage pulse at the 50 Ohm output of the MCP detector

$$V_D(t) = Q\, h_D(t) \tag{4}$$

where Q denotes the area of $V_D(t)$ and $h_D(t)$ is normalized to unit area. The actual voltage waveform V(t) at the input of the gain stage G (point 2 in Fig. 1), results from the convolution product of the detector pulse $V_D(t)$ and of the amplifier impulse response $h_A(t)$

$$V(t) = Q\, h_D(t) * h_A(t) \tag{5}$$

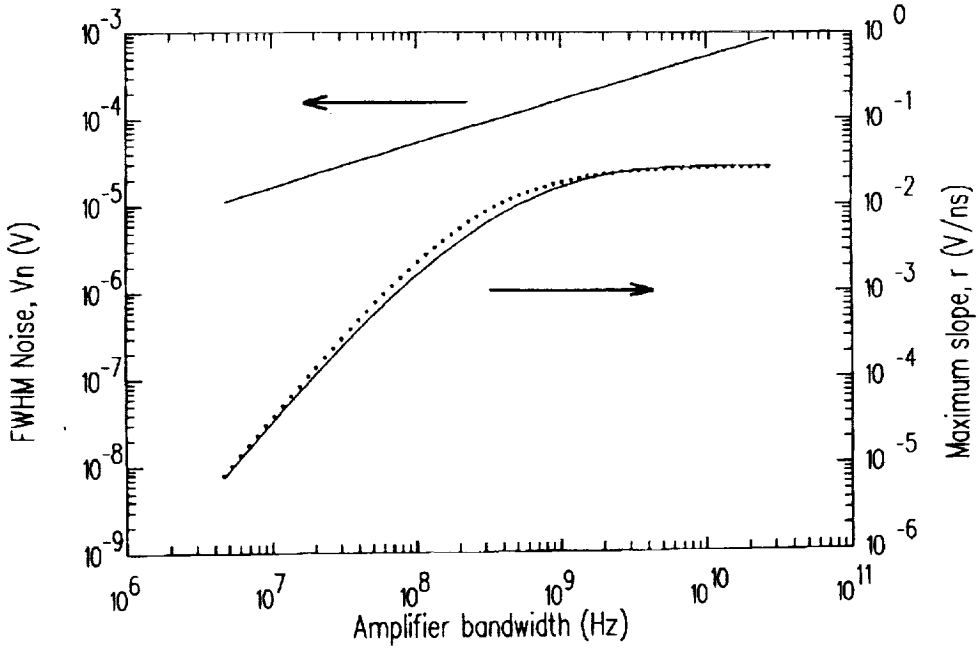

Fig.3 Maximum slope, r, of the amplified pulse and FWHM Vn of the noise amplitude distribution at point 2 in Fig.1 vs amplifier bandwidth B_A. Pulses of a 12μm channel MCP (Hamamatsu R1564U); amplifier having frequency response with two real poles, white input noise generator with rms density $a = 2nV\ Hz^{-1/2}$. Results of detailed computations of the pulse waveform (full line) are compared with the approximation discussed in Ref. [8] (dotted line).

The shape of V(t) and the corresponding maximum slope r can be obtained by numerical computations, accurately taking into account the characteristics of the detector pulse and of the amplifier impulse response [8]. A simple approximation can also be employed to obtain a sufficiently good estimate of r. Essentially, it consists in computing the slope r as result of a weighted average of the corresponding slopes of the detector pulse and of the amplifier impulse response [8]. Fig.3 reports the computed behavior of r and V_n versus amplifier bandwidth for a typical case. Fig.4 illustrates for another case the detailed behavior of the time jitter versus amplifier bandwidth. A broad minimum is found in all cases considered, centered at an optimum bandwidth value B_{Aopt} , which in all cases is well below 2GHz and mostly is around 1GHz .

The analysis carried out with a white noise spectrum leads to definite conclusions. Selecting the amplifier for very high bandwidth and paying minor attention to the noise is not only useless, but even disadvantageous. The noise has primary importance, since the time jitter is proportional to the root-mean square spectral density a. The optimum bandwidth value B_{Aopt} is markedly lower than that suggested by the criterion of keeping the risetime of the amplified pulse very near to the original risetime of the detector pulse. Even for the fastest available MCP detector, B_{Aopt} does not exceed 1.7GHz. Satisfactory results can be obtained with bandwidth values remarkably lower than B_{Aopt}, even by a factor of two. On the basis of these results, it was concluded that amplifiers employing fast bipolar transistors (BJTs) provide better performance than amplifiers based on ultrafast metal-semiconductor field-effect transistors (MESFETs). In fact, the higher bandwidth of MESFETs is not required and, working with a 50 Ohm source, the lower input current noise is not important. Furthermore, MESFETs may have higher components in the low-frequency noise spectrum. However, it must be taken into account that the input noise spectrum of BJTs also contains a high frequency component proportional to f^2. A detailed analysis [8] shows that the f^2 noise component causes a steeper increase of V_n for rising B_A, thereby shifting to lower B_A value the minimum of T_n and making much steeper the rise of T_n on the high B_A side. Fig.5 illustrates a typical case. It is worth stressing that the effect is more marked and the shift of the minimum is greater for transistors having lower white noise component (that is, lower value of a).

These results further support and enhance the conclusions drawn in the white noise analysis. The presence of a f^2 component in the noise spectrum of BJTs i) shifts to even lower value the optimum amplifier bandwidth B_{Aopt} ; ii) makes remarkably more severe the penalty for working with amplifier bandwidths higher than the optimum one ; iii) has almost negligible influence on the results obtained with amplifier bandwidth lower than B_{Aopt}.

In conclusion, the quantitative analysis demonstrates that, by using available low-noise high-frequency bipolar transistors in rationally selected operating conditions, the additional time jitter due to the circuit noise can be kept below 5 ps FWHM. In any case of interest, the behavior of the jitter versus the amplifier bandwidth can be fairly simply analyzed by using the approximate approach introduced in Ref.8. This approach just requires the knowledge of a few numerical parameters characterizing the pulse shapes involved, which can be obtained by analytical representation or by measurements of the waveforms.

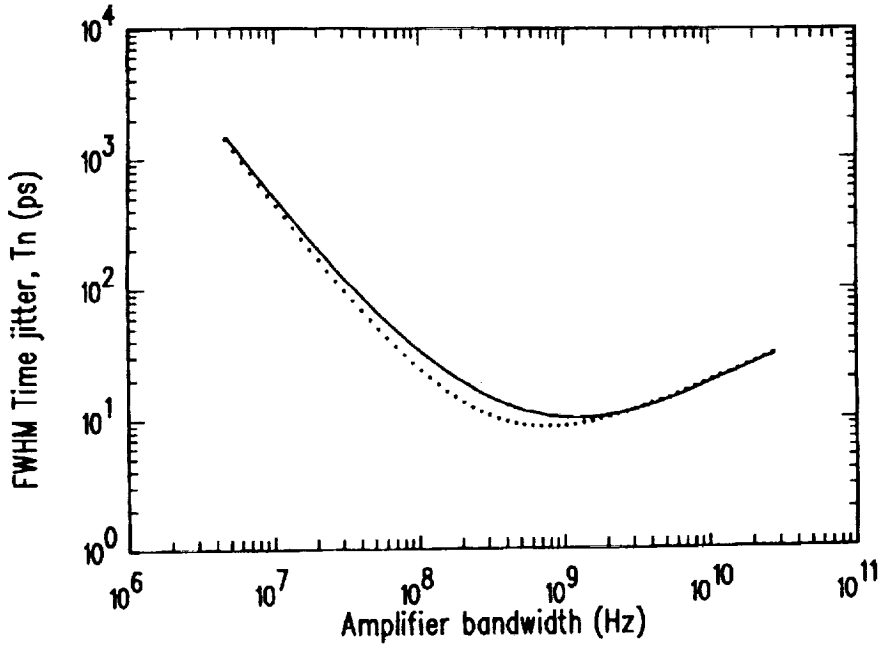

Fig.4 Additional FWHM time jitter T_n due to the noise vs amplifier bandwidth B_A, for the case of Fig.3. Results of detailed computations of the pulse waveform (full line) are compared to the approximation discussed in Ref. [8] (dotted line).

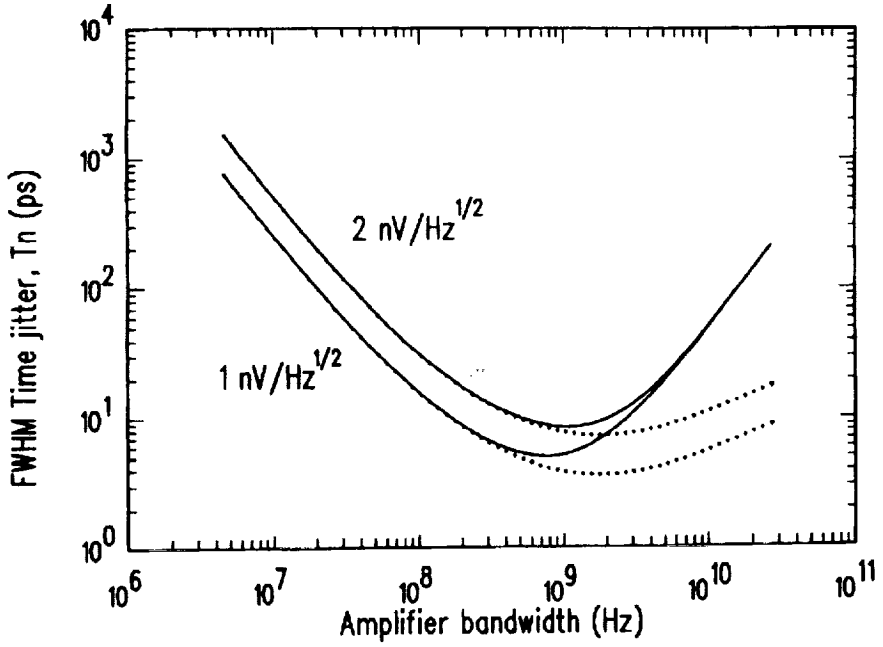

Fig.5 Effect of the f^2 spectral noise component in bipolar transistors (BJT). Pulses of a 6μm-channel MCP (Hamamatsu R2809U). Amplifier with two real poles in the frequency response, input BJT having f_T=5GHz (see Ref.8). Results with the total spectrum (full lines) are compared with those computed with only the white noise term (dotted lines) for two cases: minimum noise a=1nV $Hz^{-1/2}$ and moderately low noise a=2nV $Hz^{-1/2}$

III. CONSTANT FRACTION TRIGGERS WITH MCPs

Since single-photon pulses of photomultiplier tubes (PMTs) have statistically fluctuating amplitude, constant-fraction trigger circuits (CFT) are normally employed for accurate timing [14]. However, with the subnanosecond signals of MCPs non-ideal CFT behavior is observed. A residual amplitude-dependent time-walk sets the ultimate resolution in photon timing. A quantitative analysis of the problem has been carried out and will be here summarized [10].

Fig. 6 illustrates the basic structure and the principle of operation of a CFT circuit. The triggering point of the fast comparator is determined by the crossing of two replicas of the amplified MCP pulse, the first attenuated by a factor k, the second one delayed by a time T_D.

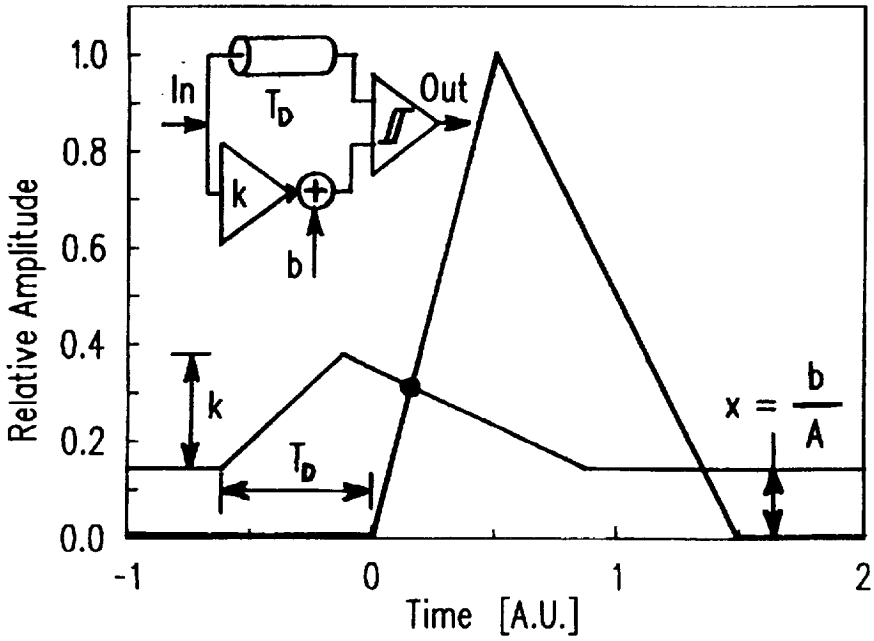

Fig.6 Working principle of Constant Faction Triggers (CFTs) based on a fast comparator with differential input. Block diagram (inset) and pulse waveforms at the comparator inputs (normalized to unit peak amplitude) are depicted in simplified form.

Crossing occurs when the delayed pulse reaches a given percentage of the peak. The time-walk effect is eliminated, since the triggering time is independent of the actual pulse amplitude A. This is strictly true only if the two waveforms have the same baseline level. However, setting both inputs at the same bias voltage level is unacceptable, since it causes the comparator to oscillate. A small dc voltage offset b is necessary; in practice, about 10 mV with modern fast comparators. This constant offset b causes a deviation from the ideal CFT operation, since it causes the crossing time to walk as A is varied. The slower is the rise of the delayed waveform, the larger is the walk. The problem is quantitatively analyzed making reference to the pulse waveform g(t) normalized at unit peak amplitude and to the correspondingly normalized baseline offset x. The pulse-amplitude distribution, with probability density p(A), is transformed in a distribution of

x, with probability density q(x).

$$x = \frac{b}{A} \tag{6}$$

$$q(x) = p(A) \left| \frac{dA}{dx} \right| = p(A) \frac{A^2}{b} \tag{7}$$

The lower threshold level A_L set for accepting the MCP pulses is translated in an upper limit x_H; conversely, the accepted maximum pulse height A_H sets a lower limit x_L. The relation between x and the time walk is readily derived. The crossing time t_c along the waveform g(t) is defined by:

$$x + k\, g(T_D + t_c) = g(t_c) \tag{8}$$

By differentiating with respect to x, we obtain:

$$dx + k \left(\frac{dg}{dt} \right)_{t_c + T_D} dt_c = \left(\frac{dg}{dt} \right)_{t_c} dt_c \tag{9}$$

Denoting by $g'_r = (dg/dt)_{t_c}$ the rising slope and by $g'_f = (dg/dt)_{t_c + T_D}$ the falling slope at the crossing point, we define the intercrossing slope

$$g'_i = g'_r - k\, g'_f \tag{10}$$

and obtain

$$dt_c = \left(\frac{dx}{g'_i} \right) \tag{11}$$

Let us denote by t_o the crossing time for x=0, which corresponds to the ideal CFT case (and is well approximated by the real CFT for pulse amplitude A much higher than the offset b). As A is decreased, the x value is increased and the crossing is shifted from t_o to a later time t_c ; the time walk t_s is $t_s = t_c - t_o$. The equation relating the time walk to x is simply obtained by integrating eq.11. The distribution of x is transformed in a distribution of t_s , with probability density $w(t_s)$. Since $w(t_s)\, dt_s = q(x)dx$ and $dt_s = dt_c$, we obtain from eq.11:

$$w(t_s) = q(x)\, g'_i \tag{12}$$

The actually observed time resolution curve $r_m(t)$ will be the convolution product of this distribution $w(t_s)$ and of the intrinsic resolution curve of the apparatus $r_i(t)$, due to other causes of time dispersion

$$r_m(t) = r_i(t) * w(t) \tag{13}$$

Since w(t) results from an inverse transformation of p(A), it is strongly asymmetric, affected by a long tail towards high t_s values. Its effect in widening the FWHM of $r_m(t)$ is therefore greater than that of a gaussian function having equal FWHM. Taking a linear pulse approximation (as outlined in Fig.6), that is, assuming constant intercrossing slope g'_i, the time walk is proportional to x and the distribution $w(t_s)$ is obtained from q(x) simply by a change of scale. It extends from a lower limit $t_{sL} = g'_i\, x_L = g'_i\, b/A_H$ to an upper limit $t_{sH} = g'_i\, x_H = g'_i\, b/A_L$. With the intercrossing slope g'_i obtained employing the suitable fast preamplifiers (risetime around 400ps, see Sec.II), a fairly small time walk effect would be estimated. For MCP types having 40ps intrinsic FWHM resolution, it would be practically negligible, since the computed FWHM of $r_m(t)$ is less than 45ps. For faster types, having 20ps intrinsic FWHM resolution, it would be moderate, since the computed FWHM of $r_m(t)$ ranges from 25 to 30ps. As a matter of fact, however, in the set-ups actually employed by the experimenters the situation significantly deviates from the linear pulse approximation. As illustrated by Fig.7, this is due to the short duration of the MCP pulses, to their shape and to the CFT setting, in particular to the minimum available value of the delay T_D.

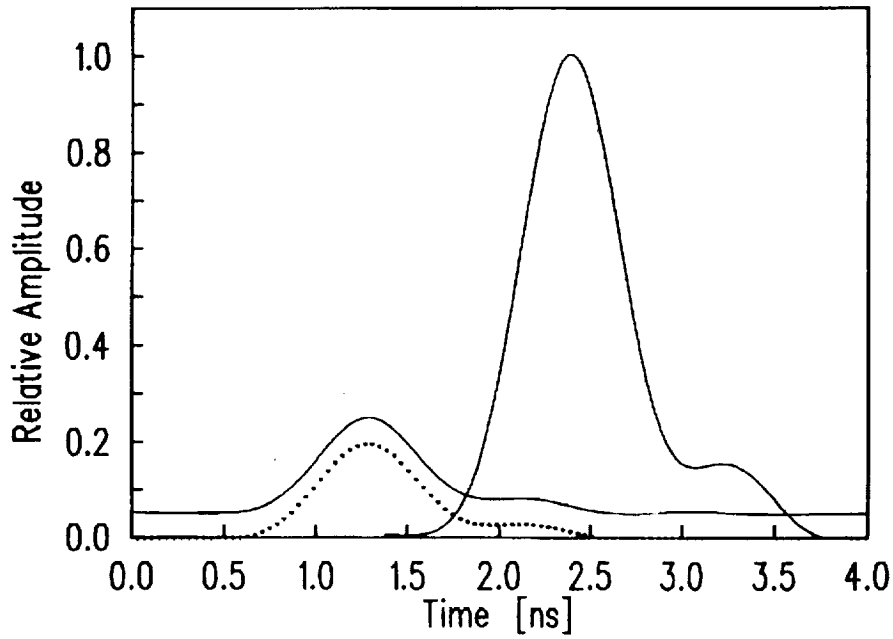

Fig.7 Pulse waveforms at the comparator inputs in the CFT, coming from a 12μm channel MCP (Hamamatsu R1564U), amplified by a HP 8447F fast amplifier. The attenuation is k=0.2, as usual in available CFTs. The delay is T_D=1.1ns, corresponding to minimal external cable length. Actual CFT operation is illustrated by the attenuated pulse with baseline offset (full line); the ideal CFT case is represented by dotted-line waveform.

The intercrossing slope g'_i is a function of the crossing time t_c and cannot be approximated by a constant in eq.s 11 and 12. The transformation from q(x) to $w(t_s)$ is no more linear and a significantly wider $w(t_s)$ results. The situation is particularly bad

when the crossing occurs at the onset of the delayed pulse leading edge, where the rise is slower and the intercrossing slope is correspondingly low. Such a situation can be avoided by making the delay T_D shorter than the duration of the input pulse. In commercial CFT circuits, T_D is mainly determined by the propagation time in a coaxial cable, externally connected to the circuit module and selected by the user. The least obtainable value of T_D is about 1.1ns or slightly less [15], determined by the connectors, the circuit layout and the minimal length possible for the external cable. This was adequate for the pulses of ordinary PMTs, lasting a few nanoseconds, but it is no more sufficient for the subnanosecond pulses of ultrafast MCPs. As illustrated in Fig.7, with T_D=1.1ns the crossing occurs just in the low slope zone of the rising waveform. The operation only roughly approximates the ideal CFT; in fact, it is intermediate between a CFT and a leading edge trigger with small, constant threshold.

Such a situation can be avoided by a suitable selection of parameters in the experiment. The analysis points out the basic criteria for minimizing the time walk effect:

i) the preamplifier gain should be high enough to keep low the value of the upper limit x_H in all cases, even when a small value of the lower threshold A_L is selected for accepting almost all pulses, e.g. 90%of the amplitude distribution p(A).

ii) the delay T_D and attenuation k should be selected for maximizing the intercrossing slope.

The latter criterion is usually not satisfied by industrially produced CFT models. Beside having too long minimum delay, they are normally set to low constant fraction values, around 0.2, which are optimal for timing signals from scintillation detectors of ionizing radiations, but not for timing single photons [10,14]. This is due to historical reasons, since CFTs were originally developed for working with ionizing radiation detectors

A detailed quantitative analysis of the CFT time-walk effect in the conditions of actual experiments can be carried out by means of computer simulation, taking accurately into account the actual shape of the signal waveform processed by the amplifier. It is worth noting that the result of the computation of the crossing time t_c versus normalized baseline offset x can be easily foreseen, by linearly shifting upwards the attenuated waveform in figures like Fig.7 and directly observing the walk of the crossing point. In the following, in order to set in evidence the effects on the time resolution, all the time distribution curves are drawn aligned at the peak value. All FWHM values reported are measured on the complete computed curve $r_m(t)$. In fact, since the shape of the distribution $w(t_s)$ is asymmetrical and far from gaussian, the FWHM value of $r_m(t)$ would be remarkably underestimated by a quadratic composition of the FWHM values of $w(t_s)$ and $r_i(t)$.

Previously published experimental results were analyzed and improvements obtainable by modifying the CFT parameters and/or the pulse shape were evaluated [10]. We first considered cases where a 12micron channel MCP Hamamatsu R1564U is employed with a fast amplifier model HP8447F. The amplitude distribution and signal waveform are reported from Yamazaki et al. [1] and from the manufacturer data sheets

and technical notes [16]. On the basis of published results [1-3] the intrinsic time distribution $r_i(t)$, due to the detector is assumed to be gaussian with 40ps FWHM.

We studied the effect of a filtering stage with a 1ns integrating time constant, interposed between fast amplifier and CFT as proposed and experimented in our laboratory [9]. The wider pulse obtained by filtering makes possible to obtain a higher intercrossing slope with the minimum delay of 1.3ns available in our set up. The computer analysis gives results in perfect agreement with the experiment, confirming that the improvement of the FWHM from 75ps to 55ps was obtained thanks to the reduction of the time walk effect.

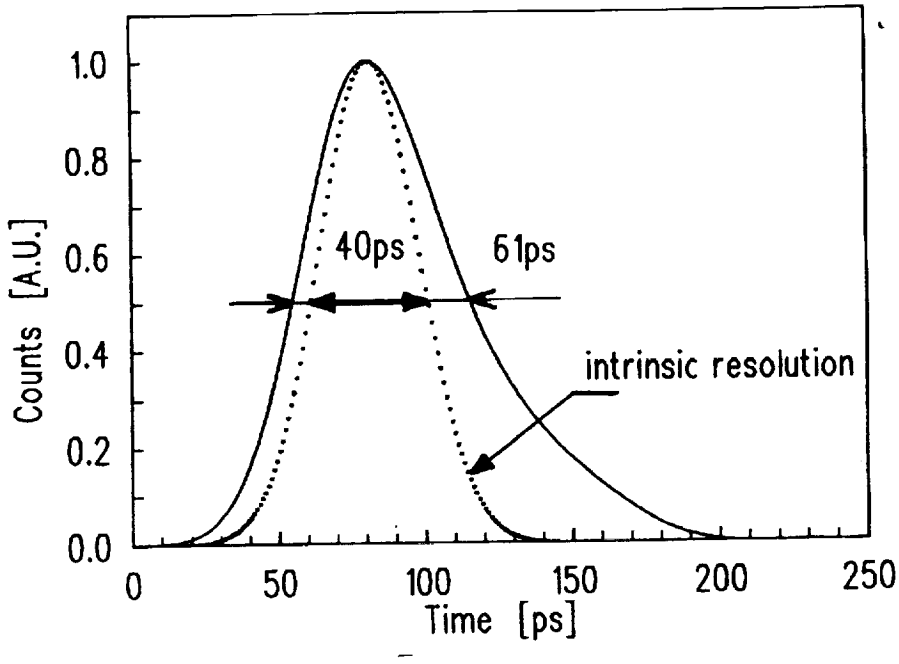

Fig.8 Computed time resolution curve for measurement with low selecting threshold level (accepting almost all pulses), compared to the intrinsic time resolution curve (dotted curve) of a 12 μm channel MCP (Hamamatsu R1564U). The computed FWHM is 61ps; the experimental value in Ref.1 is 63ps.

We analyzed then the experiments reported by Yamazaki et al. [1], where the resolution was measured with two different levels of the auxiliary lower threshold A_L of the CFT, which selects pulses accepted for the time measurement. With low threshold, accepting almost all pulses, they measured 63ps FWHM; the computed value for T_D=1.1ns and k=0.2 was 61ps, as illustrated in Fig.8. The computation also confirmed that with high threshold, accepting only 15% of the pulses, the FWHM suffers negligible degradation with respect to the intrinsic value. For the experiments with low threshold level, we also evaluated the improvement obtainable by reducing the pulse delay T_D and/or the attenuation ratio k, in order to increase the intercrossing slope. It is not difficult to reduce the delay T_D in existing CFTs, without needing to redesign and fabricate new CFT models. The available models can be modified by cutting lines in the printed circuit board and making new internal connections for a shorter delay path, that avoids the external delay cable. By modifying the resistor network that attenuates the prompt waveform (see Fig.6), one can also change the k to higher values. In order to attain k=1, however, major modifications or complete redesigning of the CFT circuit

may be necessary. The results obtained by changing the delay to T_D=0.6ns and/or the attenuation range to k=1 are summarized in Table 1.

We can conclude that with the 12 micron-channel MCP Hamamatsu R1564U it is fairly simple to reduce the time-walk effect to a tolerable or even negligible contribution.

Table 1 FWHM time resolution values obtained in the computer simulation of measurements with Hamamatsu R1564U (intrinsic FWHM resolution 40ps) and CFT circuit with low selecting threshold level (see Fig.8) and different values of the delay T_D and attenuation k.

k	0.2	0.2	1	1
T_D	1.1ns	0.6ns	1.1ns	0.6ns
FWHM	61ps	49ps	50ps	42ps

It is not strictly necessary to design new CFT models, since employing simple auxiliary circuits or making fairly simple modifications to available CFT circuits can be sufficient to the purpose. By employing a simple filter-amplifier to increase the width of the pulse fed to the CFT, without modifying the CFT circuit, the resolution widening can be reduced to less than 40%. By modifying the CFT to reduce the delay, the widening is limited to 22%. If, further to reducing the delay, the attenuation is eliminated (k=1), the widening drops to 5%. It is interesting to note that some older ZCT circuits may therefore be more suitable to single-photon timing than modern CFTs.

We may also note that the results of this analysis suggest how to select a suitable fast amplifier among a set of available models with a given value of the gain-bandwidth product, with criteria in agreement with the conclusions drawn from the analysis of the contribution of the electronic circuit noise to the time jitter. It is clearly better to select a model with moderate bandwidth (1GHz or less) and higher gain, rather than faster models with lower gain. The task of avoiding significant time-walk effect in the resolution becomes tougher with the latest and fastest MCP detectors, having 20ps or better FWHM intrinsic time resolution, such as the 6micron channel MCP model Hamamatsu R2809U. Data for the analysis of this case were obtained from Ref.3 and from the manufacturer data sheet and technical notes [16]. The intrinsic resolution curve $r_i(t)$ is assumed to be gaussian with 20ps FWHM. Since model HP8447F amplifier is very well suited also to this case [8] from the standpoint of the time jitter due to circuit noise, we analyzed set-ups employing such a fast amplifier. Fig.9 illustrates the effect of employing a shorter delay T_D in the CFT. Table 2 summarizes the improvements obtainable with modifications to the CFT circuit.

Table 2. FWHM time resolution values obtained in the computer simulation of measurements with Hamamatsu R2809U (intrinsic FWHM resolution 20ps) and CFT circuit with pulse selecting threshold level set at low level to accept almost all pulses and different values of delay T_D and attenuation k.

k	0.2	0.2	1
T_D	1.1ns	0.6ns	0.6ns
FWHM	50ps	29ps	24ps

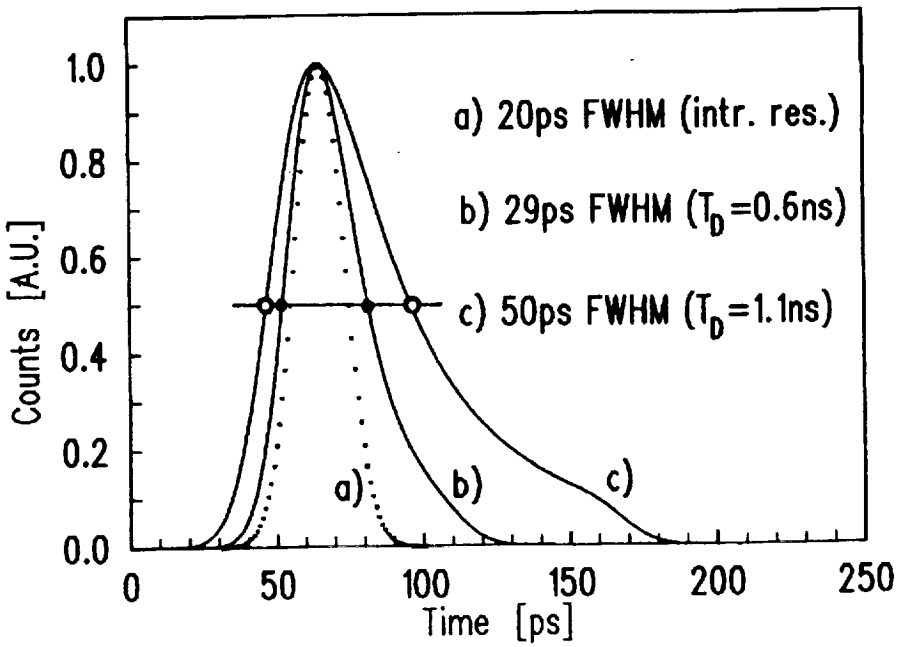

Fig.9 Computed time resolution curves, including effects of amplitude dependent time walk in CFT, for measurement set-ups with MCP model R2809U, fast amplifier HP8447F, CFT pulse selecting threshold set at low level to accept almost all pulses. The dotted curve is the assumed intrinsic resolution curve, having 20ps FWHM. Two cases are reported: a) CFT with the usual attenuation k=0.2 and delay corresponding to minimal external cable T_D=1.1ns (wider curve, 50ps FWHM); b) CFT with k=0.2, but with shorter delay T_D=0.6ns (narrower curve, 29ps FWHM).

It is interesting to compare these results to the corresponding ones for the case of the 12micron channel model R1564U. Essentially, the time walk in the corresponding situations is quite similar in the two cases, but its relative effect on the obtainable performance becomes greater as the intrinsic detector is improved. For the R2809U the actual resolution with the short delay of 0.6ns is remarkable, but 45% wider than the intrinsic one. With delay 0.6ns and no attenuation (k=1) the obtainable resolution is still 20% wider than the intrinsic. Some experimental results point out that the detector intrinsic resolution may be even better than 20ps, possibly 10ps or better.The time walk effect should therefore be considered a major limitation to the ultimate obtainable resolution.

We conclude that there is considerable margin for further improvement. Greater care should be therefore devoted to the electronic pulse processing, in order to take full advantage of the detector intrinsic resolution. It is advisable to work with CFT having k=1 and even shorter delay, possibly with specially studied filter-amplifier input stage. Designing new CFT circuits specially devised for photon counting may be rewarding.

IV. ACTIVE-QUENCHING CIRCUITS FOR SPADs

In early studies on SPADs, the bias arrangement used for the device operation was the so-called *passive quenching* circuit (PQC) [4,5,11]. This circuit employs a high load resistor (in the 100k range) in order to force the diode voltage V to drop down near to the breakdown voltage V_B after each avalanche triggering. This quenches the avalanche. The diode voltage is then slowly restored to the bias voltage, since the diode capacitance is recharged by the small current flowing through the high value resistor. The voltage recovery takes at least some microseconds. A photon can arrive during the recovery from a previous avalanche pulse and trigger the avalanche when the SPAD voltage is at some intermediate level, randomly placed between the breakdown voltage and the correct bias voltage. This has a twofold detrimental effect on the timing performance. First, the intrinsic time resolution of SPADs is strongly reduced as the excess bias voltage $V-V_B$ actually applied to the diode is reduced. Second, at lower excess bias voltage the avalanche current pulse not only has smaller amplitude, but also slower risetime. This causes a walk of the triggering time of the following timing circuit, which is not properly corrected even employing a CFT (CFTs require constant pulse shape to work properly). The intrinsic performance of SPADs can be exploited working with PQCs only in cases where the probability of such events (photons arriving during a recovery from a previous avalanche pulse) is very low, that is, where the rate of repetition of pulses is very low, at best a few kHz. Note that this limitation applies to the total rate of pulses, that is, to the sum of the dark count rate of the SPAD plus the detected photon rate, including unwanted background light.

A partial remedy to such limitations is to apply a pulsed bias voltage to simple passive circuit arrangements, for obtaining a gated operation of SPADs. The additional voltage pulse can be superimposed to the dc bias either by ac coupling or by dc coupling. The ac coupling is very simply implemented, by connecting the junction between SPAD and load resistor to a low-impedance fast pulse generator through a suitable capacitor. The dc coupled gate is obtained by employing a smaller load resistor, typically 1kOhm or less, and applying directly to it the sum of the dc bias voltage plus a pulsed additional voltage. The detailed analysis [18] of such circuit arrangements, however, points out that i) it is possible to detect not more than one photon in the gate interval ii) other specific limitations are associated to each circuit arrangement. With ac coupling, the repetition rate of gating pulses must be low. With dc coupling, the power dissipated in the SPAD may become excessive. In summary, it can be concluded that pulsed-bias passive circuits are of practical interest only for working with gate intervals having short duration, typically below 100ns, and low or moderate repetition rate.

In the early stage of development of SPADs, it became therefore clear that more sophisticated circuits were necessary, in order to fully exploit the device performance. Active quenching circuits (AQCs) were thus conceived and developed in our laboratory [6,12,13]. Essentially, the AQC performs the following operations.

i) It senses the onset of the avalanche current.

ii) It generates an output pulse, synchronous with the avalanche, with the least possible jitter.

iii) It forces the bias voltage of the diode to drop as swiftly as possible below the breakdown voltage. It must therefore have a low-impedance output driver, capable of driving efficiently the capacitance associated to SPADs and connections.

iv) Finally, it restores the initial bias after a well-controlled hold-off time, so that the diode is again ready to detect a subsequent photon. Also the reset transition must be as fast as possible, in order to reduce as far as possible the probability that a photon may arrive during the recovery of the diode voltage, with an associated degradation of the time resolution (see above).

Various problems are met for obtaining a correct AQC operation and severe requirements have to be fulfilled in order to fully exploit the available SPAD performance. A peculiar problem is caused by the large amplitude difference between the avalanche pulse generated by the SPAD and the much larger quenching pulses applied to it and reflected back at the circuit input. The AQC should be sensitive to avalanche pulses of less than 1mA (<50mV over 50), while quenching pulses have amplitude of several Volts (up to 50V in our circuits i.e. 1000 times higher than the avalanche pulse). Unless special precautions are taken in the circuit design, the AQC can be retriggered by the quenching pulse and either be latched in the triggered state or break into a self-sustaining oscillation. Another important requirement is to keep as short as possible the time from the avalanche onset to its quenching. The reason for this is twofold. First, it minimizes afterpulsing effects due to deep levels in the diode junction, acting as charge carrier traps. The charge trapped in deep levels is indeed proportional to the total avalanche charge flowing through the junction. Second, with high voltage devices, the power dissipated in the avalanching state can be fairly high and produce a remarkable variation of the device temperature, with associated variation of the breakdown voltage and of other device parameters. On the other hand, minimizing the delay between the onset of the avalanche and the arrival of the quenching voltage pulse to the SPAD is sometimes conflicting with the requirement of operating the SPAD remote from the AQC, as necessary, for instance, in order to operate a SPAD with cryogenic cooling. For a remotely operated diode, the duration of the avalanche current is inherently increased by twice the transit time in the connecting cables; that is, by 10ns per meter of connecting coaxial cable. The hold-off time must have accurately controlled duration, in order to have a well defined and controlled deadtime (avalanche time plus hold-off time). The actual value of the hold-off time can be very short, a few tens of nanoseconds or less, in cases where photons have to be counted at high rate, up to 10 MHz or more. However, in cases where photon arrival times must be accurately measured and the dark count rate must be minimized, somewhat longer hold-off time have to be employed, typically a few hundred nanoseconds, in order to avoid SPAD retriggering due to the delayed release of trapped carriers. For SPAD devices working with high excess bias voltage $V-V_B$, the quenching pulse must have large amplitude, up to 50V and possibly more, so that the transition times are limited by the slew rate attained by the quenching driver. Finally, in order to exploit the time resolution of the fastest SPADs, the jitter between the avalanche onset and the output pulse should be much lower than the intrinsic resolution of the detector, that is, it must be limited to a few picoseconds. This means that the input stage of the circuit should be designed for minimum noise. Obviously, it is not possible to fulfil at best all these requirements at the same time. Different AQC parameter setting, or even different AQC models are therefore employed for optimizing the most important performance in different cases. In our laboratory, various generations of AQC have been developed, starting in 1975 from the earliest simple model [17] and progressively increasing the performance by a steady evolution of the design [4,6,12,13,18]. Such evolution has produced an AQC design that provides remarkable flexibility for different applications and can work a SPAD in remote position (connected

by a coaxial cable) exploiting at best the device performance. With a minimum-noise input stage, the circuit has intrinsic timing jitter well below 10ps FWHM; it can work at more than 10MHz repetition rate and, with suitably designed output quenching driver, it can provide a 50V quenching pulse.

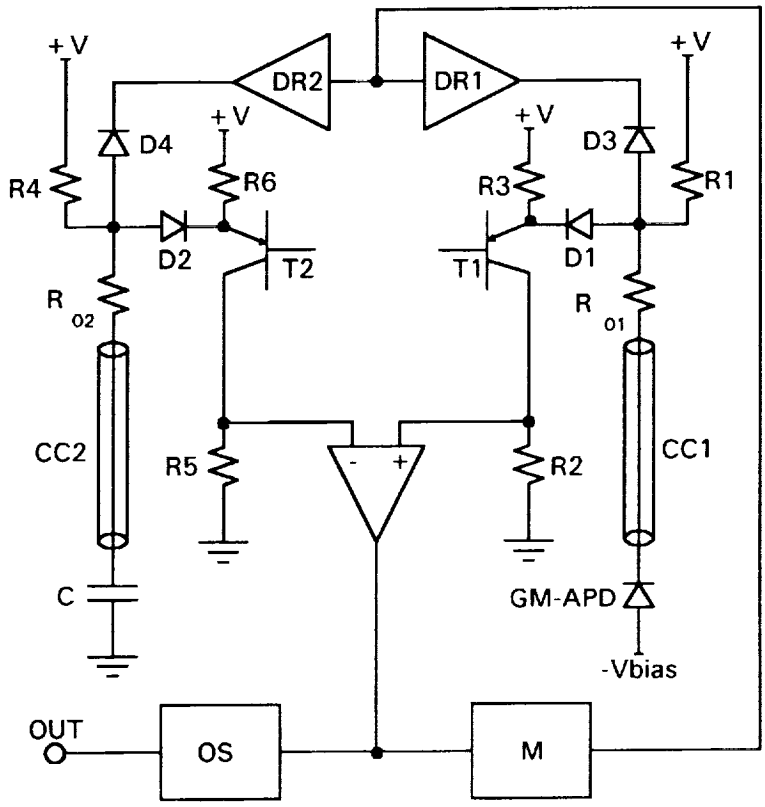

Fig.10 Simplified block diagram of the most recent AQC generation, described in the text. Note the symmetry of the circuit.

The circuit design approach, covered by international patents [13], will be here illustrated making reference to the simplified circuit diagram in Fig.7. The figure illustrates the high degree of symmetry of the circuit. Thanks to this symmetry, the fast comparator can have a low threshold level, as required to sense the avalanche pulse, and at the same time be insensitive to the quenching pulse, avoiding spurious retriggering (see above). The avalanche pulse is applied asymmetrically (only to the non-inverting terminal of the comparator): it is therefore a differential-mode signal that triggers the comparator. The quenching voltage pulse is symmetrically applied (to both input terminals of the comparator), so that it is a common mode signal and does not trigger the comparator. In order to obtain this, the symmetry should be maintained also in the voltage transients, including reflections, overshoots or ringing caused by the load connected to each circuit input. It is therefore necessary to connect to the non-inverting input of the AQC a passive load, in order to match that given by the SPAD, connected to the other input. This normally means a simple capacitor C, with capacitance value equal to that of the SPAD (a trimmer capacitor of a few pF is normally employed). In case of remote SPAD operation, care must be taken of maintaining the

symmetry by connecting with coaxial cables (CC1 and CC2) having equal length the SPAD and the matched load. The cables are terminated at the circuit inputs through the resistors R01 and R02. The avalanche signal flows through the diode D1 and the common-base transistor T1, reaching the comparator input. The role of T1 is twofold. First it establishes a low impedance input, to which the cable-matching resistor R01 is connected. Second, it provides amplification of the voltage signal fed to the comparator, which is important for minimizing the intrinsic time-jitter of the circuit, due to its electronic noise. In stationary conditions, diodes D1 (and D2) is conducting, diodes D3 (and D4) is instead not conducting. When an avalanche is triggered, the current is sensed by the comparator, whose output changes state. This signal triggers a monostable multivibrator, M, that sets the duration of the quenching pulse. In order to obtain the desired amplitude of the quenching signal, a suitable voltage driver stage, DR, is employed. When the quenching voltage pulse is applied by DR, the voltage through D3 becomes direct, the diode conducts and the quenching pulse reaches the photodiode. At the same time the diode D1 is driven to reverse bias condition and prevents the high voltage pulse (up to 50V) from reaching T1. If diode D1 were not present, the entire quenching pulse would be applied to the base-emitter junction of T1, causing it to break down. Another important effect of the two diodes is to break the positive feedback loop of the circuit, thus reducing the risk of oscillations. The AQC output pulse is derived from the comparator, through an output stage OS.

By employing this kind of AQCs, the timing performance of SPADs has been verified down to 20ps FWHM [5]. The flexibility and performance of the circuit have been extensively tested in many different experiments, carried out in a wide variety of conditions, with SPAD working either embedded in the circuit or remote from it and operating in different ambients over a wide range of device temperatures, including cryogenic cooling.

ACKNOWLEDGMENTS

Work supported in part by ASI (Italian Space Agency), CNR (Italian National Research Council) and MURST (Italian Ministry of University and Research). The author wish to thank N.Carbone and S.Masci for their technical support in the development of Active Quenching Circuits.

REFERENCES

1 I.Yamazaki, M.Tamai, H.Kume, H.Tsuchiya and K.Oba, Rev. Sci. Instrum **56**, 1187 (1985).

2 D.Bebelaar, Rev.Sci.Instrum. **57**, 1116 (1986).

3 H.Kume, K.Koyama, K.Nakatsugawa, S.Suzuki, and D.Fatlowitz, Appl. Opt. **27**, 1170 (1988).

4 S.Cova, G.Ripamonti and A.Lacaita, Nucl. Instrum. Methods **A253**, 482 (1987).

5 S.Cova, A.Lacaita, M.Ghioni, G.Ripamonti, T.A.Louis, Rev. Sci. Instrum. **60**, 1104 (1989).

6 S.Cova, A.Longoni, and A.Andreoni, Rev. Sci. Instrum. **52**, 408 (1981).

7 A.Lacaita, S.Cova, M.Ghioni, Rev. Sci. Instrum. **59**, 1115 (1988).

8 S.Cova, M.Ghioni, and F.Zappa, Rev. Sci. Instrum. **62**, 2596 (1991).

9 S.Cova and G.Ripamonti, Rev. Sci. Instrum. **61**, 1072 (1990).

10 S.Cova, M.Ghioni, F.Zappa, and A.Lacaita, Rev. Sci. Instrum. to be published.

11 R.H.Haitz, J. Appl. Phys. **35**, 1370 (1964); **36**, 3123 (1965).

12 S.Cova, A.Longoni, and G.Ripamonti, IEEE Trans. Nucl. Sci. **NS-29**, 599 (1982).

13 S.Cova, US.Patent #4,963,727, Italian patent 22367A/88. Industrial licence to SILENA S.p.A. Milano (Italy).

14 P.W.Nicholson, *Nuclear Electronics* p. 259 (J.Wiley, NewYork, 1974).

15 See e.g. Instruction Manual of ORTEC Mod.583 or Tennelec Mod.454.

16 Hamamatsu Photonics K.K., Hamamatsu City, Japan, and Hamamatsu Corp., Bridgewater, N.J. U.S.A., MCP-PMTs data sheets and Technical Informations No. ET-03/Oct.1987.

17 P.Antognetti, S.Cova and A.Longoni, Proc. Ispra Nucl. Electron. Symp. 1975, Euratom Publication **EUR 537e**, 453 (1975)

18 S.Cova et al. Rev. Sci. Instrum. to be published

N94-15570

Tracking capabilities of SPADs for laser ranging

F. Zappa, G. Ripamonti+, A. Lacaita*, S. Cova*, and C. Samori**

* Politecnico di Milano, Dipartimento di Elettronica and CEQSE-CNR,
Piazza L.da Vinci, 32 - 20133 Milano (Italy)

+ Università degli Studi di Milano, Dipartimento di Fisica,
Via Celoria, 16 - 20133 Milano (Italy)

ABSTRACT

The spatial sensitivity of Single-Photon Avalanche Diodes (SPADs) can be exploited in laser ranging measurements to finely tune the laser spot in the center of the detector sensitive area. We report the performance of a SPAD with 100μm diameter. It features a time resolution better than 80ps rms when operated 4V above V_b at -30C, and a spatial sensitivity better than 20μm to radial displacements of the laser spot. New SPAD structures with auxiliary delay detectors are proposed. These improved devices could allow a two dimensional sensitivity, that could be employed for the design of pointing servos.

I. INTRODUCTION

Due to their high quantum efficiency and picosecond time resolution, Single-Photon Avalanche Diodes (SPADs) are gaining acceptance as detectors for laser ranging experiments. In SPADs the onset of the avalanche current, triggered by a photogenerated carrier, marks the photon arrival time. We have recently demonstrated that not only the timing information, but also the position of the photon absorption can be extracted from the avalanche current rising edge, by exploiting the physical mechanisms involved in the device operation [1]. Measurements previously performed on a position-sensitive SPAD with 14μmx140μm rectangular sensitive area showed that these structures are capable of time resolution better than 30ps rms and spatial resolution better than 5μm rms [1].

In this paper we suggest to exploit the position-sensitive capability of SPADs to keep the echo signal from the satellite always in the center of the detector sensitive area. First, we briefly recall the operation of these novel detectors. Then, we discuss the performance of a circular device (100μm diameter) large enough to make possible the first alignment of the telescope and the subsequent tracking of the satellite. Auxiliary electrodes could be used to obtain position sensitive detectors with angular measurement capability.

II. OPERATION OF SPAD POSITION SENSITIVE DETECTORS

Recently, the avalanche dynamics in silicon SPADs has been investigated; high performance detectors have been designed and fabricated [2-4]. To the purpose of our discussion, here we briefly recall the basic operation of SPADs with a depletion layer only a few microns thick [5]. The avalanche photodiode is operated biased above the breakdown voltage, V_b, but no current flows until the first carrier triggers the avalanche in a seed point. Then, the free carrier concentration swiftly rises by impact ionization around the seed point and, in a few tens of picoseconds, the free carrier space charge lowers the local multiplication rate to a self-sustaining level. The carrier density around the seed point cannot increase further, unless the avalanche is triggered in the surroundings by lateral diffusion of avalanching carriers. As the activated area increases, the diode current rises. At the end, when the multiplication process occurs over the whole active area, the avalanche current reaches the final steady state value given by the ratio of the excess bias above V_b and the diode series resistance.

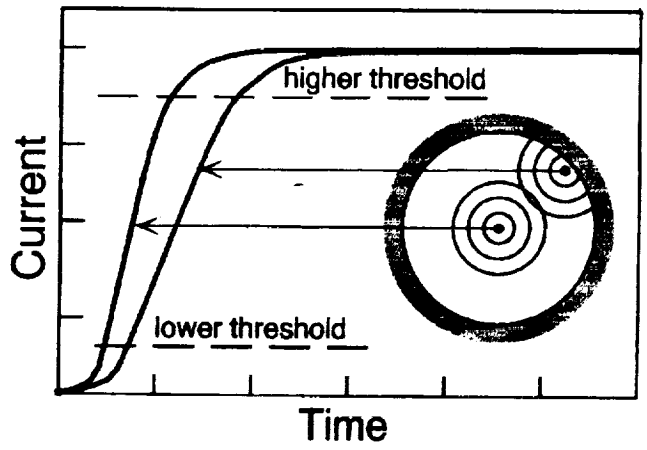

Fig. 1 Avalanche dynamics in a circular device: the curves qualitatively show the dependence of the current rise on the point where the avalanche is triggered. The circle schematically represents the sensitive area of the detector with spreading avalanches. The delay between the crossing times of the two thresholds is proportional to the current rise-time.

The pulse crossing of a discriminator threshold gives the timing information. However, this peculiar dynamics causes the avalanche pulse leading edge to depend on the position where the avalanche is triggered. Fig.1 schematically shows the rise of the diode current in a circular device. The closer is the seed point to the center, the faster is the activation of the whole sensitive area. Therefore, the current leading edge becomes steeper as the seed point moves from the periphery to the detector center. This effect sets a limit to the timing performance of the detector [2,3], but it can also be exploited to get the position

information: the shape of the avalanche leading edge carries the spatial information on the point where the photon was absorbed [1].

III. EXPERIMENTAL DATA

Fig.2 shows the cross section of the tested devices. The avalanching region is the n^+p^+ junction: the depleted region is about 1μm thick. The electric field at the edge is tailored by the n^+p junction with the epilayer. A complete discussion of the structure is carried out in Ref.6. The detector has a 100μm diameter and a V_b of 14.3V.

The rise time of the avalanche current pulses was accurately measured by an Active Quenching (AQ) circuit [7] with two discriminators having different thresholds. The purposes of the AQ circuit are: i) to sense the onset of the avalanche current; ii) to lower the bias of the photodiode below the breakdown voltage, thus quenching the avalanche; and iii) to rapidly restore the bias after a suitable dead time to enable the detection of another photon. The first discriminator is set to sense the avalanche when the current is still low (0.4mA), while the second is triggered when the avalanche is almost saturated. The delay between the output pulses of the discriminators gives the rise time of the avalanche pulse.

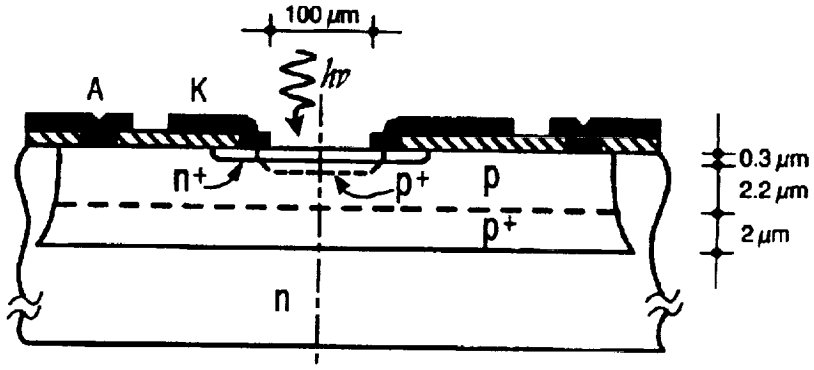

Fig.2 Cross section of the double epitaxial devices tested in the experiments. The active n^+p^+ junction is built in a 10 Ωcm p epistrate. The buried p^+epilayer is 0.3 Ωcm.

In order to reduce the dark count rate, the detector was cooled by a Peltier stage at -30C and operated in gated mode: in stand-by the diode was reverse biased below V_b, and a waveform generator provided pulses at 10 kHz, raising the bias 4V above V_b for 500ns. A 850nm laser diode synchronously emitted a 20ps rms optical pulse, focused to a 10μm spot with a microscope. A Time to Pulse Height Converter measured the delay between the triggering times of the two discriminators. A histogram of the measurements was collected with a MultiChannel Analyzer.

We carried out various measurements by changing the radial position of the light spot. Fig.3 shows the histograms of the delay between the threshold crossing times. The peak shifts 130ps when the laser spot moves from the center to the edge of the detector. The

inset of Fig.3 shows the complete dependence of the peak shift on the spot position. As the laser spot shifts more than 20μm from the device center, the histogram peak moves considerably and a suitable feedback system can react to restore the original centered position.

The time resolution of the device was measured just by recording the delay between the laser shot and the crossing time of the low threshold discriminator. The observed resolution changed somewhat with focusing and with the position of the spot. With the light focused to a 10μm spot size in the center of the sensitive area, the time resolution was 80ps rms.

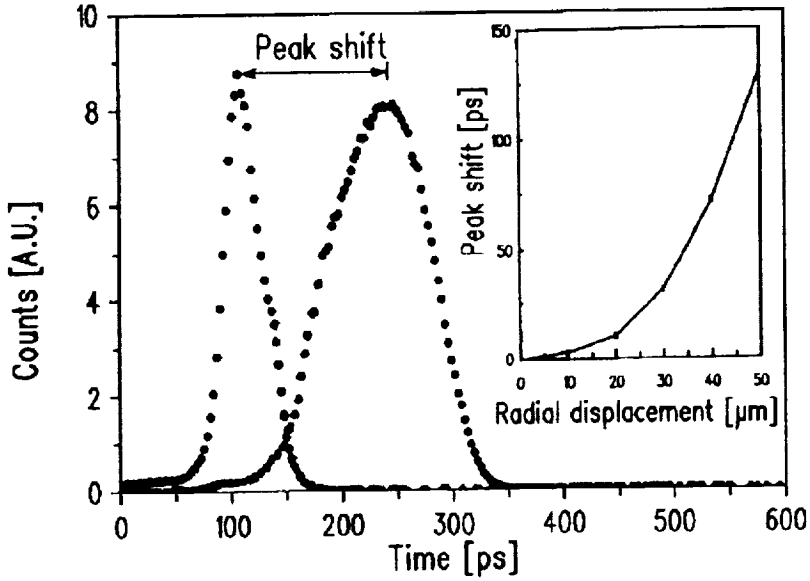

Fig.3 Avalanche pulse rise-time, measured as the delay between the crossing times of the low and the high thresholds of Fig.1. The two histograms correspond to the measurements performed by focusing the laser spot in the center (first histogram to the left) and at the edge of the detector of Fig.2 (histogram to the right). The peak shifts 130ps when the laser spot moves to the periphery of the detector. The inset shows the complete dependence of the peak shift on the spot position.

It is worth noting that photons absorbed at the same distance from the device center generate avalanche pulses with the same risetime. Therefore, these devices cannot give the information on how to operate in order to position the light spot in the detector center, in a single measurement. A trial and error method should be adopted to keep centered the echo light signal.

Fig.4 describes a possible improvement of the technique in order to achieve a complete angular sensitivity. Four SPAD sensors are placed along two perpendicular axes of the main detector, close enough to its boundary to be triggered when the avalanche reaches the corresponding edge. Since the avalanche spreads evenly from the seed point, by measuring the time delay between the current pulses of the sensors one can get the position of the laser

spot over the main sensitive area. Pointing servos could be implemented to correct for misalignement, thus keeping the laser spot always in the center of the main photodetector. It is worth noting that the design of such a device is expected to be critical in the coupling between the delay detectors and the central SPAD. Projects are under way in our laboratories to study suitable stuctures and the most effective coupling arrangements.

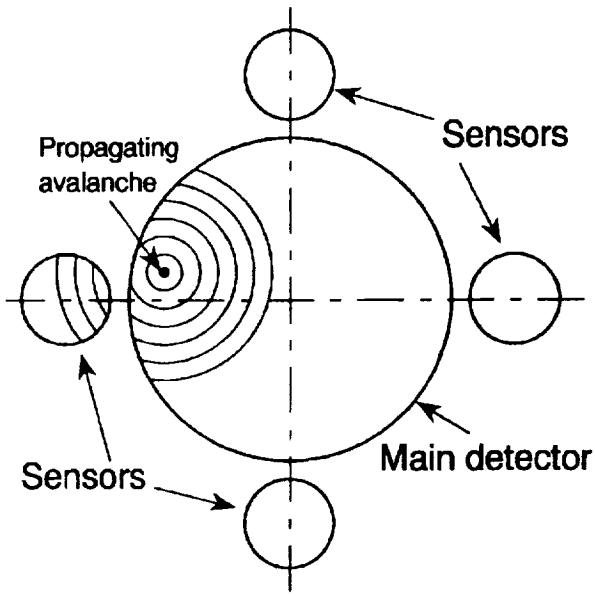

Fig.4 Proposed improvement of the position sensitive detector in order to achieve a complete angular sensitivity. Four SPADs can sense when the avalanche reaches the edge of the central device. By measuring the time delay between the current pulses of the sensors, one can obtain the position of the laser spot over the main sensitive area.

IV. CONCLUSIONS

A position-sensitive single-photon detector with 100μm diameter has been demonstrated. It features a time resolution better than 80ps rms when operated 4V above V_b at -30C, and a spatial sensitivity better than 20μm to radial displacements of the laser spot. The detector provides a continuous sensitive area, free from dead zones, and can be exploited in laser ranging measurements to keep the laser signal always centered into the sensitive area. We have also proposed a more complex SPAD structure, where the introduction of auxiliary delay detectors could allow a complete angular sensitivity of the device. These structures are investigated to overcome the trial and errors method used in pointing with simple position-sensitive SPADs.

ACKNOWLEDGEMENTS

Work supported in part by ASI (Italian Space Agency), CNR (Italian National Research Council) and MURST (Italian Ministry of University and Research). The authors wish to thank ST-Microelectronics for the fabrication of the samples, and S. Masci for his technical support.

REFERENCES

1. G. Ripamonti, M. Ghioni, S. Cova, and M. Mastrapasqua, *IEEE Electron Device Lett.* **EDL-13**, 35 (1992).

2. A. Lacaita, M. Mastrapasqua, M. Ghioni, and S. Vanoli, *Appl. Phys. Lett.* **57**, 489 (1990).

3. A. Lacaita and M. Mastrapasqua, *Electron. Lett.* **26**, 2053 (1990).

4. A. Lacaita, F. Zappa, S. Cova, G. Ripamonti, and A. Spinelli,: *8th International Workshop on Laser Ranging Instrumentation.* Annapolis, MD, May 18-22, 1992

5. S. Cova, A. Lacaita, M. Ghioni, G. Ripamonti, and T.A. Louis, *Rev. Svi. Instrum.* **60**, 1104 (1989).

6. A. Lacaita, M. Ghioni, and S. Cova, *Electron. Lett.* **25**, 841 (1989).

7. S. Cova, A. Longoni, and G. Ripamonti, *IEEE Trans. Nucl. Sci.* **NS-29**, 599 (1982).

N94-15571

How to squeeze high quantum efficiency and high time resolution out of a SPAD

A. Lacaita, F. Zappa*, S. Cova*, G. Ripamonti+ and A. Spinelli**

* Politecnico di Milano, Dipartimento di Elettronica and CEQSE - CNR,
Piazza L. da Vinci, 32 - 20133 Milano (Italy)

+Università degli Studi di Milano, Dipartimento di Fisica,
Via Celoria, 16 - 20133 Milano (Italy)

ABSTRACT

We address the issue whether Single-Photon Avalanche Diodes (SPADs) can be suitably designed to achieve a trade-off between quantum efficiency and time resolution performance. We briefly recall the physical mechanisms setting the time resolution of avalanche photodiodes operated in single-photon counting, and we give some criteria for the design of SPADs with a quantum efficiency better than 10% at 1064nm together with a time resolution below 50ps rms.

I. INTRODUCTION

Solid state photodetectors nowadays employed in laser ranging applications fall into two categories: reach-through avalanche photodiodes (APDs) with a depletion layer about $30 \div 200\mu$m thick [1-3], and shallow junction APDs with a depletion layer about 1μm thick [4-6]. The former are commercially available devices designed for low noise operation in optical communications, while the latter, called Single-Photon Avalanche Diodes (SPADs), are specifically designed for timing applications.

In laser ranging measurements reach-through APDs show several advantages over ordinary Photomultiplier Tubes (PMTs): i) At the operative bias the photodiode is fully depleted and the depletion layer, tens of microns thick, leads to a quantum efficiency higher than 30% at the Nd-YAG emission wavelength. ii) A time resolution of 150ps rms has been demonstrated with RCA C30902S: this value favourably compares with the timing performance of PMTs [7]. iii) The sensitive area diameter (500μm or more) is large

enough to make possible the alignment of the telescope and the subsequent tracking of the satellite.

Indeed, high performance SPADs can attain much better time resolution (8ps rms) [4]. However, these devices have a quantum efficiency lower than 1% at 1064nm and their small active area (5μm diameter) makes impossible their use in laser ranging measurements.

In this paper we address the issue whether a silicon SPAD can be suitably designed to achieve a trade-off between quantum efficiency and time resolution performance. We briefly recall the physical mechanisms setting the time resolution of APDs operated in single-photon counting. We discuss how the performance depends on the device geometry and the junction electric field profile. We give some criteria for the design of SPADs with a quantum efficiency higher than 10% at 1064nm and a time resolution below 50ps rms. This combination of performance cannot be achieved with any commercially available single photon detector, both solid state and vacuum tube.

II. AVALANCHE PHYSICS AND TIME RESOLUTION

Single photon sensitivity is achieved with APDs operated biased above the junction breakdown voltage, V_b. At this bias a single photogenerated carrier can trigger a diverging avalanche process. The leading edge of the avalanche current marks the photon arrival time [1-6]. Any jitter in the delay between photon absorption and the crossing time of the discriminator threshold, impairs the precision in timing measurements [4-6].

The ultimate limit to the timing resolution of a SPAD comes from the thickness of the depletion layer. In fact, the distance between the point where the photon is absorbed and the junction leads to a statistical delay between the photon absorption time and the avalanche triggering. As a rule of thumb, if the photon absorption length, L_a, is longer than the depletion layer thickness, W, and carriers drift at the saturated velocity (v_s=10ps/μm) almost everywhere in the depleted region, the ultimate rms time jitter will be of the order of $W/(3.5v_s)$=2.9ps rms per each depleted micron. Since in silicon the absorption length, L_a, of a photon at 1064nm is 83μm, the choice of a 10μm depletion layer thickness guarantees a quantum efficiency higher than 10%, with an ultimate time resolution less than 30ps rms. Unfortunately, other mechanisms do not allow to reach this limit.

In the device operation the avalanche is triggered by photon absorption in a seed point, then it progressively spreads over the whole detector area. The leading edge of the diode current is affected by the spreading process. In SPADs, with thin depletion layer and small active volume, the avalanche spreads evenly from the seed point to the remaining detector area by transverse diffusion of avalanching carriers [5,6]. This mechanism makes the avalanche propagating with a transverse velocity given by [5]:

$$v_p = 2\sqrt{D/\tau} \tag{1}$$

where D is the average transverse diffusion coefficient of the carriers and τ is the time constant of the avalanche build-up, which increases by increasing the device bias.

Fig.1 helps in understanding how the avalanche spreading impairs the timing performance. In fact, the closer the seed point is to the center of the junction area, the faster is the activation of the whole device. Therefore, in the circular device shown in

Fig.1, the current leading edge becomes steeper as the seed point moves from the periphery to the center. Since a photon can be absorbed everywhere on the detector area, this effect causes a randomness in the pulse crossing of the timing threshold. It follows that the achievable time resolution is related to the difference, Δ, between the crossing times of the fastest and the slowest current pulses. This difference increases by increasing the sensitive area and/or decreasing v_p (i.e. the bias).

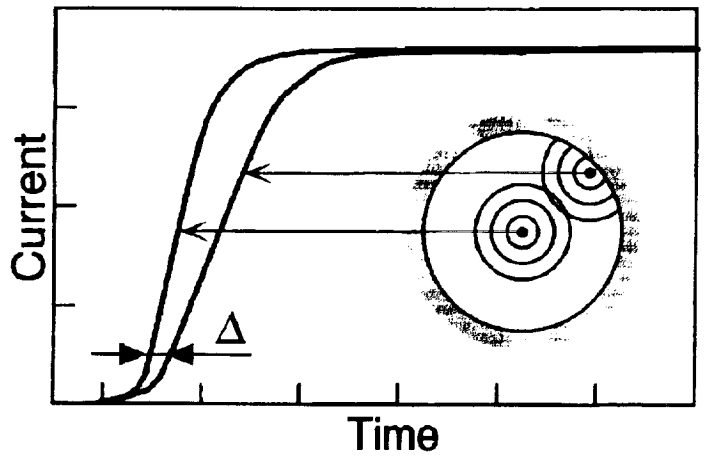

Fig.1 Avalanche dynamics in a circular device: the shift Δ between the crossing times of the fastest and the slowest leading edges sets the limit to the time resolution of the detector. The inset schematically shows the sensitive area of the detector with concentric circles representing the spreading avalanche.

As the detector volume increases, another phenomenon can play a role in the avalanche propagation. Secondary photons, emitted by hot carriers radiative relaxation processes in the avalanching region, can be absorbed in other regions, thus triggering the avalanche even there. Photons with absorption length of a few hundred microns are the most effective in sowing the avalanche. This latter process is dominant in APDs with large sensitive area and thick depletion layer [3].

We have developed a computer simulation of the avalanche dynamics. Fig.2 shows a comparison between the current leading edge of a RCA C30902S APD biased 40V above V_b at room temperature and the result of the computer program. It is worth noting that, due to the intrinsic randomness of the photon-assisted process, the timing performance of the device (170ps rms) is considerably worst than the ultimate limit set by the 30μm thick depletion layer. Moreover, the time dispersion increases by increasing the level of the timing threshold.

In order to reach a reasonable trade-off between quantum efficiency and time resolution, the impairing effects of the photon-assisted spreading have to be overcome. In principle this goal can be achieved in two ways: i) by adopting a timing threshold low enough to sense the avalanche current soon after the avalanche triggering and before the emission of

the first secondary photon; ii) by designing the detector structure so that the lateral carrier diffusion becomes the steering mechanism of the avalanche spreading. The design of fast and sensitive detector circuits is under way in our laboratories. In the next section, we will give some guide-lines on the design of high quantum efficiency SPADs with the avalanche propagation steered by transverse carrier diffusion.

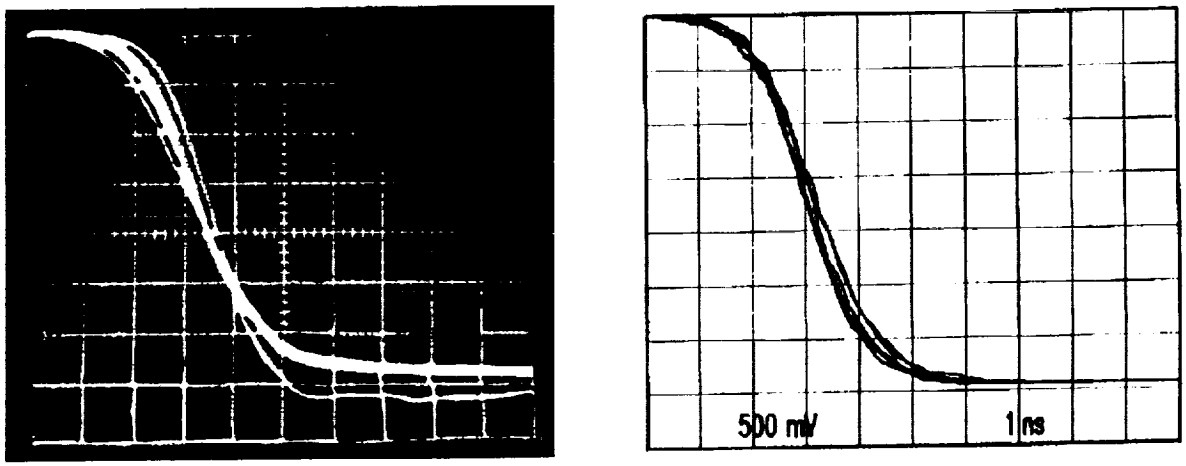

Fig.2 Comparison between the current leading edge of a RCA C30902S APD biased 40V above V_b at room temperature (left) and the result of the computer simulation of the avalanche dynamics (right).

III. DESIGN CRITERIA

In order to make it clear some fundamental design rules, let us compare the expected performance of two devices with 10% quantum efficiency at 1064nm. Therefore, both devices are supposed to have a 10μm depletion layer thickness. The inset of Fig.3 shows the electric field profile of the first device (D#1) at 169V, that is 34V above the estimated V_b=135V. The peak electric field is 3.3x10^{5}V/cm. The high field region is about 3μm thick and, in the remaining part of the depletion layer, the electric field (6x10^{4}V/cm) makes the carriers drifting at saturated velocity. The second device (D#2) has a similar electric field profile (inset of Fig.3) but a high field region only 0.3μm thick and an estimated V_b of 63V. Since the two devices have different V_b, we will compare their performance at the same relative excess bias $(V_0-V_b)/V_b$. Thus D#2 will be operated at 79V and the peak electric field will be 6x10^{5}V/cm.

Fig.3 shows the dependence on the device radius of both diffusion and photon assisted spreading velocities, as obtained from a computer simulation of the avalanche dynamics. The diffusion velocity was estimated from Eq.(1), while the photon assisted contribution was estimated by switching off the diffusion process in the simulation, and then computing the resulting ratio between the device radius and the current risetime. As expected, the role of the photon-assisted process increases by increasing the sensitive area radius; it becomes

eventually dominant in D#1 for a radius greater than 80μm. D#2 has a diffusion velocity more than three times larger and a photon assisted process less effective than in D#1.

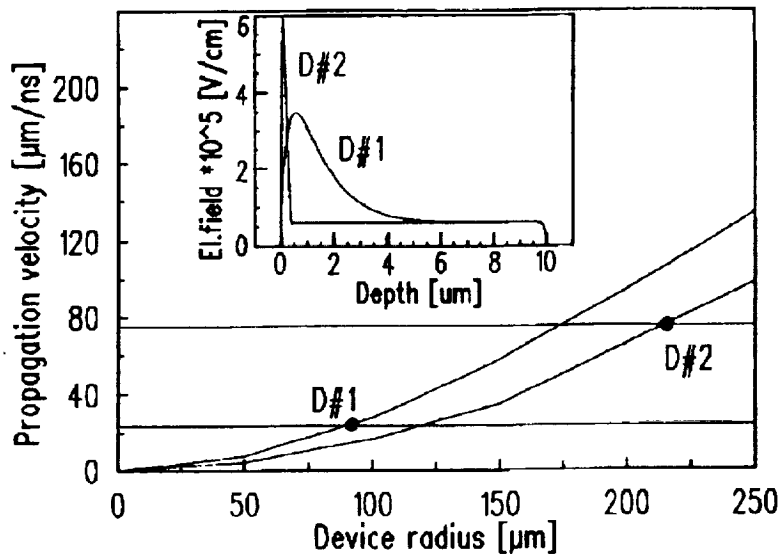

Fig.3 Dependence of the diffusion and the photon assisted spreading velocities on the device radius. as obtained from a computer simulation of the avalanche dynamics in two devices with a 10μm thick depletion layer. The inset shows the electric field profiles assumed in the calculations.

The higher diffusion velocity is due to the steeper electric field profile of D#2. In fact, the avalanche time constant, τ, is proportional to the carrier transit time in the high field region and is inversely proportional to the loop gain of the avalanche feedback process (i.e. the average number of impact ionization events experienced by a carrier crossing the junction). It can be shown that two junctions with similar electric field profile have the same avalanche loop gain when biased at the same relative excess bias. Therefore, in the present comparison, the devices are operated at the same loop gain, and the thinner high field region of D#2 results in a correspondingly shorter multiplication time constant, τ. From Eq.(1) it follows that D#2 is expected to have a faster diffusion-assisted avalanche propagation.

With regard to the difference in the photon-assisted process, it should be noted that D#2 is supposed to work at only 16V above V_b, while D#1 is operated at 34V excess voltage. Both of them have the same depletion layer thickness and therefore the same series resistance. It follows that, at the supposed operating conditions, the current flowing through D#2 is less than that of D#1. Since the photon emission rate is proportional to the current, the photon assisted propagation is less effective in D#2.

These results highlight that, by adopting a suitable steep electric field profile, the diffusion-assisted avalanche propagation can overcome the noisy photon-assisted process even in large area SPADs. We estimated the time resolution of a SPAD detector with 100μm diameter and the electric field profile of D#2 as follows. We computed the leading

edge of the avalanche pulses triggered at the center and at the edge of the detector, assuming that the avalanching area spreads evenly with a radial velocity of 75μm/ns. The time resolution is expected to be proportional to the difference, Δ, between the crossing times of the fastest and the slowest avalanche pulses. By using a timing threshold at 0.3mA, we forecast Δ=87ps. Therefore the time resolution of such a device, defined as the rms value of the timing curve, should be better than 50ps.

IV. CONCLUSIONS

We have discussed the physical mechanisms setting the timing resolution of Single-Photon APDs. In present devices, the timing resolution is limited by the mechanisms involved in the avalanche spreading from the seed point to the entire sensitive area. The best time resolution is obtained when the steering mechanism is the multiplication-assisted diffusion. We have shown that, with a proper design of the electric field profile, the diffusion-assisted process can overcome the photon-assisted spreading also in APDs with a large sensitive area. Therefore, SPAD devices with time resolution better than 50ps rms and a quantum efficiency better than 10% at 1064nm could be obtained. In such devices, the timing resolution would be ultimately limited by the transit time in the thick depleted region.

ACKNOWLEDGEMENTS

Work supported in part by ASI (Italian Space Agency), CNR (Italian National Research Council) and MURST (Italian Ministry of University and Research). The authors wish to thank ST-Microelectronics for the fabrication of the SPADs; EG&G Optoelectronics for providing the reach-through APDs; and S. Masci for his technical support.

REFERENCES

1. P.P. Webb, R.J .McIntyre, and J. Conradi, *RCA Rev.* **35**, 234 (1974).

2. A. Lacaita, S. Cova, and M. Ghioni, *Rev. Sci. Instrum.* **59**, 1115 (1988).

3. M. Ghioni and G. Ripamonti, *Rev. Sci. Instrum.* **62**, 163 (1991).

4. S. Cova, A. Lacaita, M. Ghioni, and G. Ripamonti, *Rev. Sci. Instrum.* **60**, 1104 (1989).

5. A. Lacaita, M. Mastrapasqua, M. Ghioni, and S. Vanoli, *Appl. Phys. Lett.* **57**, 489 (1990).

6. A. Lacaita and M. Mastrapasqua, *Electron. Lett.* **26**, 2053 (1990).

7. D. Bebelaar, *Rev. Sci. Instrum.* **57**, 1116 (1986).

THE SOLID STATE DETECTOR TECHNOLOGY FOR PICOSECOND LASER RANGING

I.Procházka

Faculty of Nuclear Science and Physical Engineering,Czech Technical University
Brehova 7, 115 19 Prague, 1 Czechoslovakia
phone/fax +42 2 848840, telex 121254 fjfi c, E-mail tjean@csearn.bitnet

GENERAL

The millimeter accuracy, multiple wavelength laser ranging to the satellite and long ground baseline is a goal for nineties. Assuming the laser, optics and electronics technology currently available, the optical detectors represent the principal contributions to the ranging error budget in the laser ranging chain. In our group we developed an all solid state laser ranging detector technology [1,2,3], which makes the goal of millimeter accuracy achievable. Our design and construction philosophy is to combine the techniques of : single photon ranging, ultrashort laser pulses and fast fixed threshold discrimination while avoiding any analog signal processing within the laser ranging chain.

The all solid state laser ranging detector package consists of the START detector and the STOP solid state photon counting module. Both the detectors are working in an optically triggered avalanche switching regime. The optical signal is triggering an avalanche current buildup which results in the generation of an uniform, fast risetime output pulse. The fixed threshold discrimination represents no drawback for our application. In connection with the ultrashort laser pulses (35 picoseconds or less), this detection technique introduces the timing jitter of a few picoseconds on the multi photon signal level and less than 15 picoseconds on a single photon signal level. Omitting the fast analog signal processing is simplifying the ranging system and simultaneously increasing its temporal stability.

START DETECTOR PACKAGE

It detects a small portion of the laser output and triggers the time interval unit. The detection structure on silicon is used. The detector is operating in an avalanche switching regime, it is acting as a fixed threshold opto switch generating on its output an uniform current pulse. Its amplitude is typically 8 Volts, length 5 nanoseconds, the risetime is bellow 400 picoseconds. Thanks to the output pulse shape and its uniformity, no additional pulse amplification and discrimination is needed. As no analog signals are propagating along the cables, the detector output is uniform and its amplitude is high, the whole setup is highly resistant to the radio frequency interference and electrical noise problems. This fact is becoming significant in the vicinity of a laser system generating a lot of electrical noise. The detector is capable of operation in three modes :

1. In **linear mode** it may be used as a laser output pulse monitor with the bandwidth of 1 GHz.

In this mode, the optical alignment of the detector may be optimized.
2. The **opto switching mode** described above is used for ranging.
3. In the **self oscillation mode** the detector generates on its output the sequence of uniform output pulses with the repetition rate of about 1 kHz. This mode is and attractive feature for test purpose.

The detector jitter contribution to the overall jitter budget was not measured independently. When it has been used to trigger the streak camera, the overall trigger jitter (detector + streak camera) of 8-16 picoseconds has been observed using the passively mode locked lasers with pulse length 3 - 100 psec FWHM. Thus, the trigger jitter contribution of the START detector itself is well bellow 15 picoseconds for these pulse lengths. Generally, in connection with the active-passive mode locked lasers with pulse lengths bellow 100 psec and the fast response time interval unit input, the jitter contribution of the START detector may be neglected.

SOLID STATE PHOTON COUNTING MODULE

It is used to detect the laser ranging echo signals. The Module is a self consistent detector package, which detects single photons of light over the wavelength range from 0.35 to 1.1 microns. The Module utilizes a unique silicon Single Photon Avalanche Diode (SPAD) [4,2], which is connected in the active quenching and gating circuit and pulse biased above the break. Biasing the diode above the break, the extreme gain of order of 1.10^9 is achieved. This high gain obtained within the semiconductor chip permits to avoid any further amplification of the detector output and the constant fraction discrimination, as well. Simple fixed threshold discrimination technique is used to recognize the detector output and to generate the uniform output NIM pulse. The detector may be gated using the TTL signal, the 'gate on' delay is bellow 25 nanoseconds. The detection diode together with the active quenching circuit, the gating logic, the discriminator, output pulse forming circuit and the light collecting optics in enclosed in one package. It is a cylinder, 120 millimeters long, 40 millimeters in diameter. The optics has an effective focal length 10 millimeters and is optimized for the beam diameter of 8-10 millimeters. Due to the diode relatively small sensitive area (20, 40 or 100 micrometers), the resulting receiver field of view is limited. Using the 100 micrometer diameter diode and the final collecting optics f/D=1, the resulting field of view is 40 arc seconds when installed in the 0.5 meter input aperture telescope. Using the same diode in connection with the 1 meter aperture telescope, the 20 arc seconds field of view is achieved. The 40 um detection chip has been successfully used for SLR at Helwan and Graz, however, the field of view has been to narrow for routine operation. Due to the detection and avalanche buildup mechanisms inside the SPAD chip, the minimal

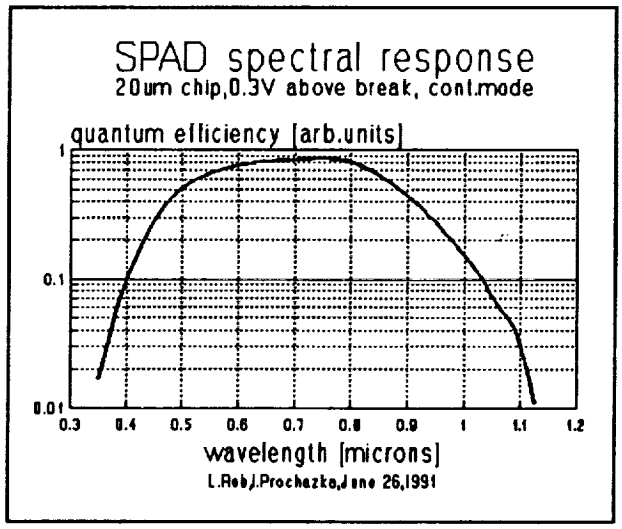

Figure 1 The SPAD relative photon detection probability, 0.3V above the break, + 25°C

detection jitter is achievable when the input photons are focussed on a small spot near to the diode's center. Thus, the good quality light collecting and beam focussing optics together with a careful optical alignment is essential for minimal jitter.

The photon detection probability and its dependence on the wavelength has been measured using the 20 um diameter diode operating in the continuous counting mode. The diode was biased 0.3 Volt above the break. The results are plotted on Figure 1. The detection probability depends on the diode biasing, it increases with the increase of the bias up to 3 Volts above the break. For higher biases, the photon detection probability is not increasing more. The absolute figures of the quantum efficiency have been estimated by comparison to the calibrated photocathode to be 20 % at 0.53 um wavelength and bias 3 Volts above the break. Using the calibrated light source and filters, the quantum efficiency exceeding 20 % at 0.8 um wavelength and biased only 1V above the break has been observed [5].

DETECTORS PERFORMANCE

Since the last Workshop presentation [6], the detectors overall performance has been improved. The SPAD manufacturing technology has been tuned to get lower dark count rates. This is permitting to apply higher voltages above the break and hence to get lower jitter, lower time walk and higher photon detection probability, as well. The active quenching and gating logic has been modified (Prochazka, Kirchner) for this purpose. Cooling the diode using the Peltiere elements down to -25 Centigrades [7] the reduction of the dark count rate is achieved. This proved to be useful for ranging to low satellites suffering of the poor range prediction. Both the detectors are routinely used at the Satellite Laser Station in Graz, Austria since 1989. Most of the application results are based on the data acquired at this site.

The SPAD detector timing jitter and its dependence on the diode biasing is plotted on Figure 2. The jitter values have been computed on the basis of the ground target ranging at the 0.53 um wavelength. At the same figure, the effective dark count rate at the temperatures +25 and -10 Centigrades is plotted. The jitter is depending on the wavelength, it is slightly increasing toward longer wavelengths and reaches 60-70 picoseconds at the 1.06 um when the SPAD is biased 2.5V above the break. The detector package time walk, the detection delay dependence on the signal strength is plotted on Figure 3. The data have been acquired biasing the diode 2.5 Volts above the break and using the semiconductor laser pulser 32 psec FWHM. On Figure 4 there is a plot of evolution of the ranging system single shot precision using the all solid state detector technology together with the list of main upgrades. The ranging system temporal stability is demonstrated on Figure 5, where is a plot of the mean values of ground target calibration runs. It is worth to mention, that this test has been made at the time, when the system single shot precision was 8-9 millimeters. The drift of the 5 picoseconds per hour may be attributed to the

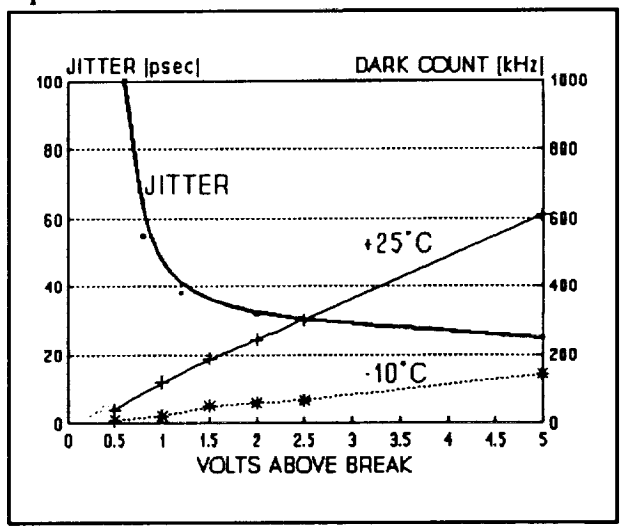

Figure 2 SPAD detector package jitter and effective dark count rate at +25°C and -10°C

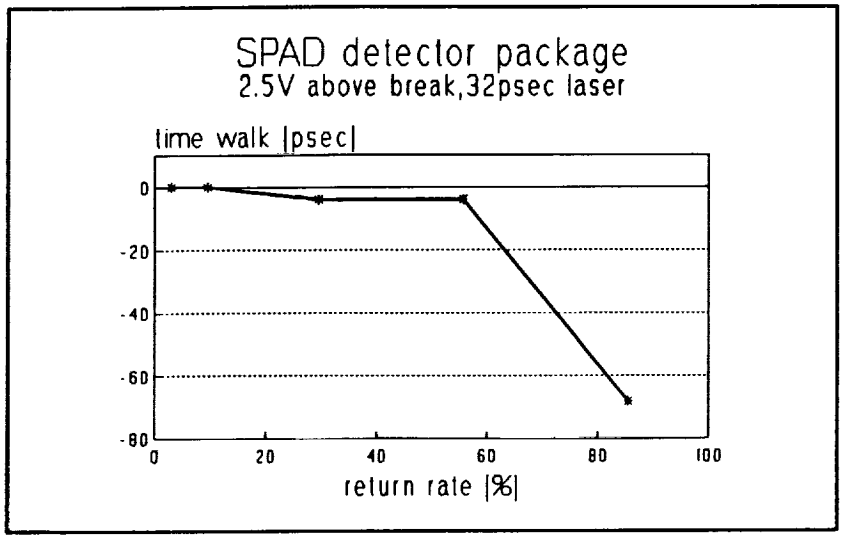

Figure 3 SPAD time walk test,2.5V above break,32 psec laser

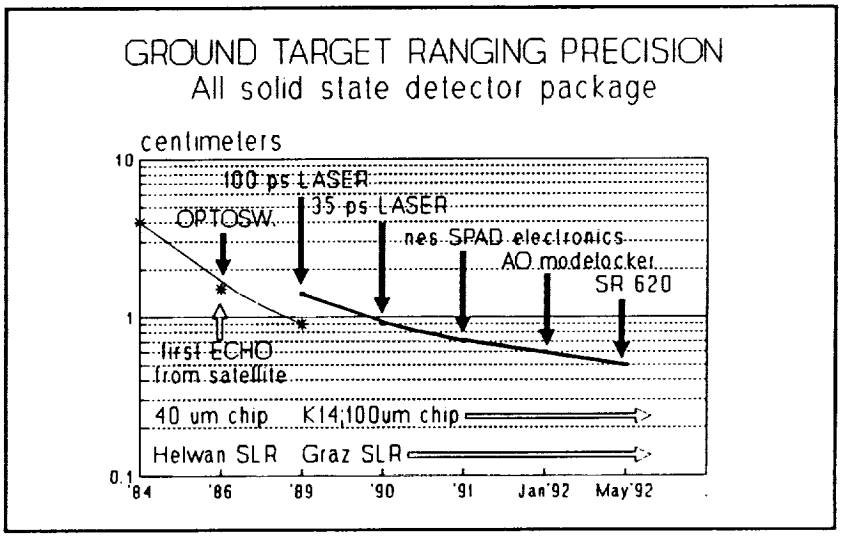

Figure 4 Ground target ranging precision increase

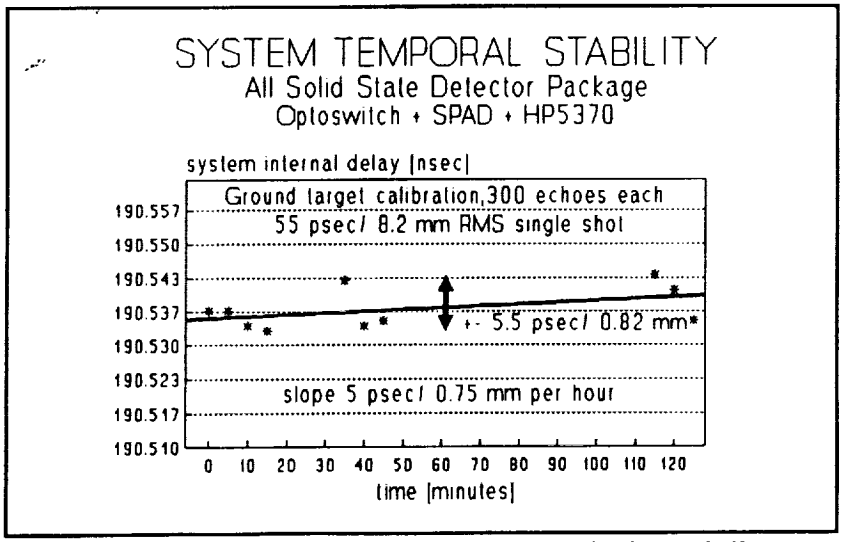

Figure 5 System temporal stability, vert.scale 1mm / div

temperature changes within the control & electronics room and its influence on the ranging counter.

SATELLITE RANGING RESULTS

The all solid state detector package has been used for routine satellite laser ranging since early 1989. Since that time, the ranging precision has been improved from original 2 centimeters to subcentimeter level in 1992.

The satellite signature - its contribution to the echo signal time spread is becoming dominant in the ranging error budget when using the 35 psec laser pulse and single photon detection. On a single photon echo signal level, the ranging precision is limited to 1.5 cm when ranging to Starlette, to 2 cm for Lageos and to 4-5 cm when ranging to Etalon satellites. The effect of the "satellite depth" may be reduced by the use of multiphoton (1-10) return signal strength. In this case, the return photon(s) reflected from the first corner cube is detected. As the detector response time is bellow 20 picoseconds, the photons reflected by the more distant corner cubes are not contributing and are not affecting the detection and discrimination process. Due to this effect, the satellites may be ranged with the return rate exceeding 95% without a detectable time walk and the satellite signature effect on the ranging jitter reduced.

The typical ranging precision obtained in Graz is 8 millimeters for Starlette and ERS-1 satellites, 10 millimeters for Lageos and 12-15 millimeters for Ajisai satellites.

CONCLUSION

The field use of the solid state detector package for satellite laser ranging at various sites over the world : Graz Austria, RGO Great Britain, Shanghai China, MTLRS-1 Germany proved the top performance of the solid state detector technology. The extremely simple, compact and rugged design, the absence of the analog signal processing and the resulting subcentimeter ranging capability and submillimeter temporal stability are the most attractive features. The optical alignment of the SPAD is a difficult task, but it may be solved once the receiver optics is properly designed. The satellite signature and its influence on both the random and systematic error budget is becoming significant from the point of view of millimeter ranging goal.

REFERENCES

[1] I.Prochazka,proc.of 6th Int.Work.on Laser Ranging Instrumentation, Antibes, Sept.1986
[2] K.Hamal,I.Procházka,B.Sopko,G.Kirchner,proc.of Conference on Lasers and Electro Optics, CLEO'90, Anaheim, CA, May 1990
[3] I.Procházka et al,proc.VIIth International Symposium on Ultrafast Processes in Spectroscopy, Bayreuth, Germany, October 1991
[4] S.Cova et al,JQE, Vol.19,630 (1983)
[5] J. Říčka, M.Hoebel, private communication, (1992)
[6] I.Prochazka,K.Hamal,B.Sopko,proc.7th Int.Workshop on Laser Ranging Instrumentation, Matera, Italy, Oct. 1989
[7] G.Kirchner, private communication (1991)

STREAK CAMERA BASED SLR RECEIVER FOR TWO COLOR ATMOSPHERIC MEASUREMENTS

Thomas Varghese, Christopher Clarke, Thomas Oldham, Michael Selden
Allied Signal Aerospace Company,
BFEC/CDSLR
10210 Greenbelt Road
Seabrook, MD 20706 USA

Abstract.

To realize accurate two-color differential measurements, an image digitizing system with variable spatial resolution was designed, built and integrated to a photon-counting picosecond streak camera, yielding a temporal scan resolution better than 300 femtosecond/pixel. The streak camera is configured to operate with 3 spatial channels; two of these support green (532 nm) and uv (355 nm) while the third accommodates reference pulses (764 nm) for real-time calibration. Critical parameters affecting differential timing accuracy such as pulse width and shape, number of received photons, streak camera/imaging system nonlinearities, dynamic range, and noise characteristics were investigated to optimize the system for accurate differential delay measurements.

The streak camera output image consists of three image fields, each field is 1024 pixels along the time axis and 16 pixels across the spatial axis. Each of the image fields may be independently positioned across the spatial axis. Two of the image fields are used for the two wavelengths used in the experiment, the third window measures the temporal separation of a pair of diode laser pulses which verify the streak camera sweep speed for each data frame. The sum of the 16 pixel intensities across each of the 1024 temporal positions for the three data windows is used to extract the three waveforms. The waveform data is processed using an iterative three-point running average filter (10 to 30 iterations are used) to remove high-frequency structure. The pulse pair separations are determined using the half-max and centroid type analysis. Rigorous experimental verification has demonstrated that this simplified process provides the best measurement accuracy. To calibrate the receiver system sweep, two laser pulses with precisely known temporal separation are scanned along the full length of the sweep axis. The experimental measurements are then modelled using polynomial regression to obtain a best fit to the data. Data aggregation using normal point approach has provided accurate data fitting techniques and is found to be much more convenient than using the full rate single shot data. The systematic errors from this model has been found to be less than 3 ps for normal points.

TWO COLOR ATMOSPHERIC MEASUREMENTS

Objectives:

- Measure atmospheric velocity dispersion difference between 532 and 355 nm using short (≤30 ps) pulses, very accurately (2-3 ps).
- Compute atmospheric refraction correction (RC) directly from the differential range.
- Compare this correction with the theoretical one obtained from surface meteorological measurements for agreement/refinement.

Issues of Importance:

- Is there true hydrostatic equilibrium in the troposphere on a local scale ?
- What are the diurnal and seasonal effects ?
- What effect does the local/global temperature gradient have on RC ?

STREAK CAMERA SLR RECEIVER SYSTEM

Desirable Features:

- High Temporal Resolution (ps).
- Good temporal sweep stability.
- High quantum efficiency (> 10%)
- Single photoelectron sensitivity.
- High resolution spatial imaging (< 1 ps/pixel).
- Repetition Rate ≥ 10 Hz.
- Optical calibration source with temporal and amplitude stability.
- Spectral filtering and wavelength isolation.

STREAK CAMERA CHARACTERISTICS

Streak Tube

- Manufactured by Hamamatsu; model C2909, streak tube N2666.
- Sweep: linear
- Maximum MCP gain ≃ 10^6
- Spectral response: 200 - 850 nm
- Phosphor Screen: P20
- Effective Photocathode size: ≃6mm

Input Optics

- Spectral transmission: 200 - 1600 nm
- Transmission efficiency: 65% (350 - 1100 nm)
- Image magnification: 1:1
- Effective F-value: F/4.5

Output Optics

- Image magnification: 1:1
- Effective F-value: F/1.2

Photocathode gating characteristics

- Duration: 0.3 - 100 μs
- Extinction: 10^3

Timing Characteristics

- Maximum sweep ≃ 250 ps/12 mm
- Trigger jitter < 10 ps
- Temporal resolution: 1.4 ps (MCP gain = 1)
- Dynamic range: (30:1 at high gain)

READOUT CHARACTERISTICS

- Vidicon - Plumbicon (North American Philips model 88 X Q)
- Preamplifier gain: ≤80 dB
- Raster Control: flexible, current operation 1024 (time) X 128 (horizontal)
- Sampling rate: 1 M sample/second (max = 16 Msample/second)
- Maximum data transfer to computer: ≃ 700 Kbytes/second (MC-DIO-32)
- Maximum rate (currently) limited by interface card 9.4 Hz
- Maximum Temporal Resolution/pixel: 250 fs
- Data windowing: 3 windows for 3 wavelengths, each operating with 1024 X 16 pixels

TWO COLOR DIFFERENTIAL MEASUREMENT
THEORETICAL AND EXPERIMENTAL LIMITS OF ACCURACY

$$R_0 = R(\lambda_1) - \frac{c}{2}\left\{\left[\frac{f(\lambda_1)}{f(\lambda_2)-f(\lambda_1)}\right]\left[(T_0+T(\lambda_2)) - (T_0+T(\lambda_1))\right]\right\} \quad (1)$$

$$\sigma^2_{R_0} = \sigma^2_{R(\lambda_1)} + \left\{\left[\frac{c}{2}\right]\frac{f(\lambda_1)}{f(\lambda_2)-f(\lambda_1)}\right\}^2 \sigma^2_{\delta T(\lambda_1,\lambda_2)} \quad (2)$$

Where

$$\delta T(\lambda_1,\lambda_2) \triangleq T(\lambda_2)-T(\lambda_1)$$

$$\sigma_{\delta T(\lambda_1,\lambda_2)} = \sqrt{\sum_{i=1}^{2}\left[\frac{\Delta T^2(\lambda_i)\ S(\lambda_i)}{n_{ph}(\lambda_i)\cdot\eta_{QE}(\lambda_i)\cdot A}\right] + \left[\sigma^2_{MCP} + \sigma^2_{sweep}\right]} \quad (3)$$

R_0	=	Absolute range to the satellite
$R(\lambda)$	=	Measured range at wavelength λ
$f(\lambda)$	=	Dispersion factor
T_0	=	Absolute time of flight
$T(\lambda)$	=	Increase in time of flight through atmosphere at wavelength λ
$S(\lambda)$	=	Pulse profile factor
η_{ph}	=	Number of photons
η_{QE}	=	Photocathode quantum efficiency
A	=	Microchannel coupling factor
δT	=	Differential time of flight
σ	=	Standard deviation
$\Delta T(\lambda)$	=	Pulse width at λ

DATA ANALYSIS TECHNIQUES

SMOOTHING (3 POINT) ALGORITHM

$$\langle I_p \rangle^{(m)} = \frac{\left[a\langle I_{p-1} \rangle^{(m-1)} + b\langle I_p \rangle^{(m-1)} + c\langle I_{p+1} \rangle^{(m-1)} \right]}{(a + b + c)} \quad (4)$$

$$\langle I_0 \rangle^{(m)} = \frac{\left[b\langle I_{1022} \rangle^{(m-1)} + c\langle I_1 \rangle^{(m-1)} \right]}{(b + c)} \quad (5)$$

$$\langle I_{1023} \rangle^{(m)} = \frac{\left[a\langle I_{1022} \rangle^{(m-1)} + b\langle I_{1023} \rangle^{(m-1)} \right]}{(a + b)} \quad (6)$$

$\langle I_p \rangle^m$ = Mean intensity of the pixel at location p after "m" iterations

a,b,c = Weighting coefficients

DETECTION:

- Peak
- Half Maximum (Mean Value)
- Centroid

ORIGINAL PAGE
BLACK AND WHITE PHOTOGRAPH

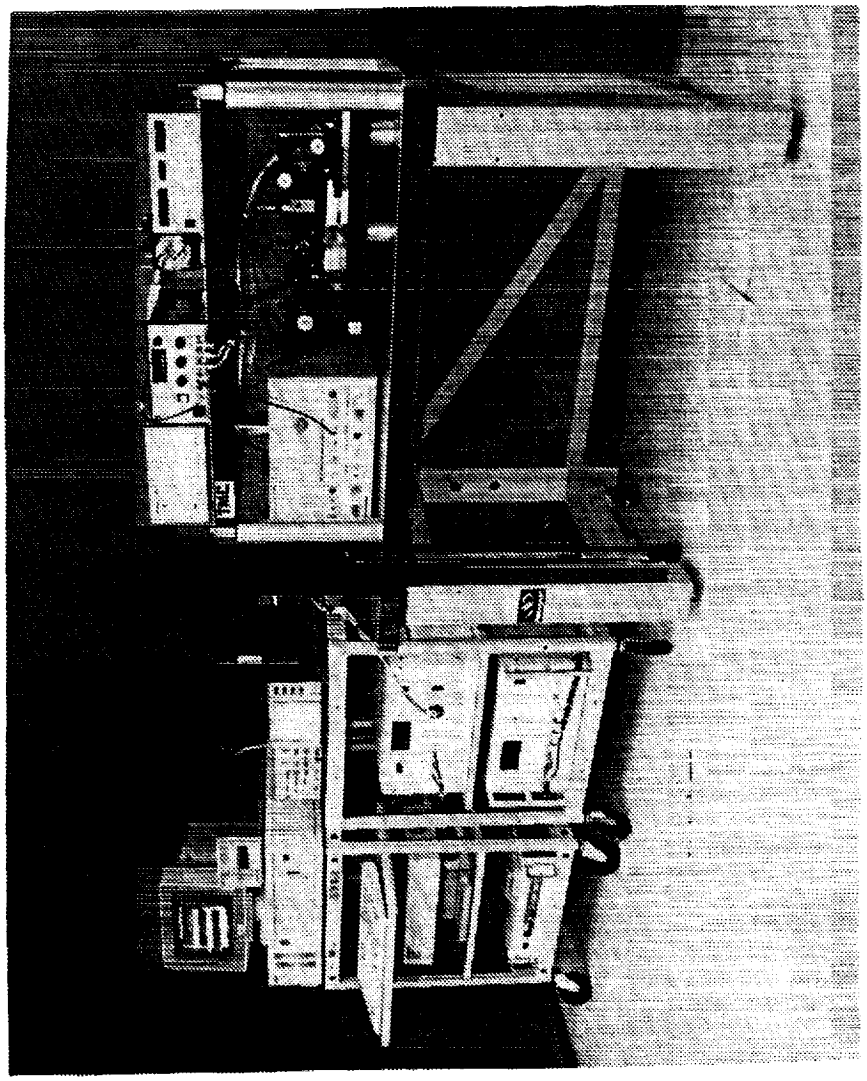

PHOTOGRAPH OF THE STREAK CAMERA BASED SLR RECEIVE SYSTEM.

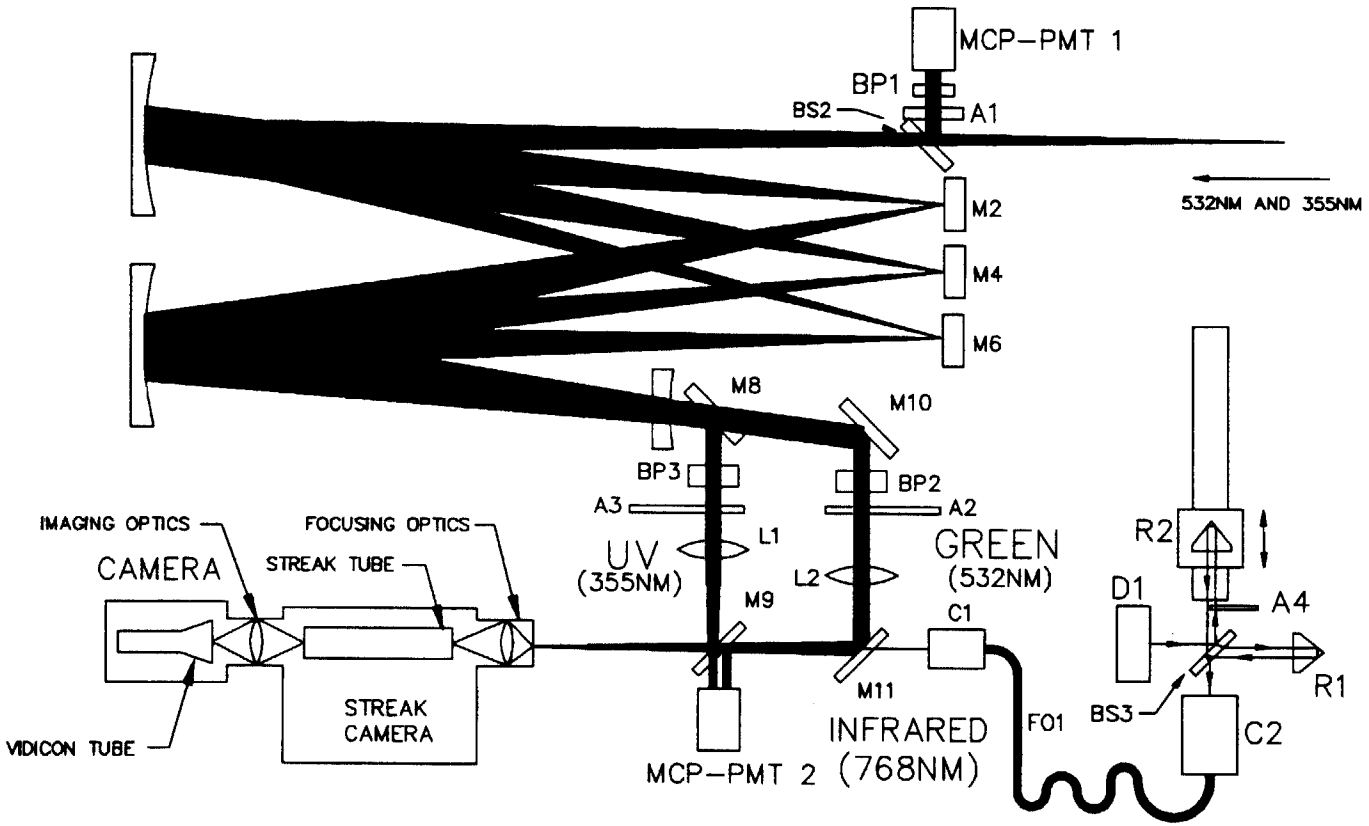

OPTICAL SCHEME OF THE STREAK CAMERA RECEIVER SYSTEM, CURRENTLY USED FOR TWO COLOR MEASUREMENT WITH THE NASA GSFC 1.2 METER TELESCOPE.

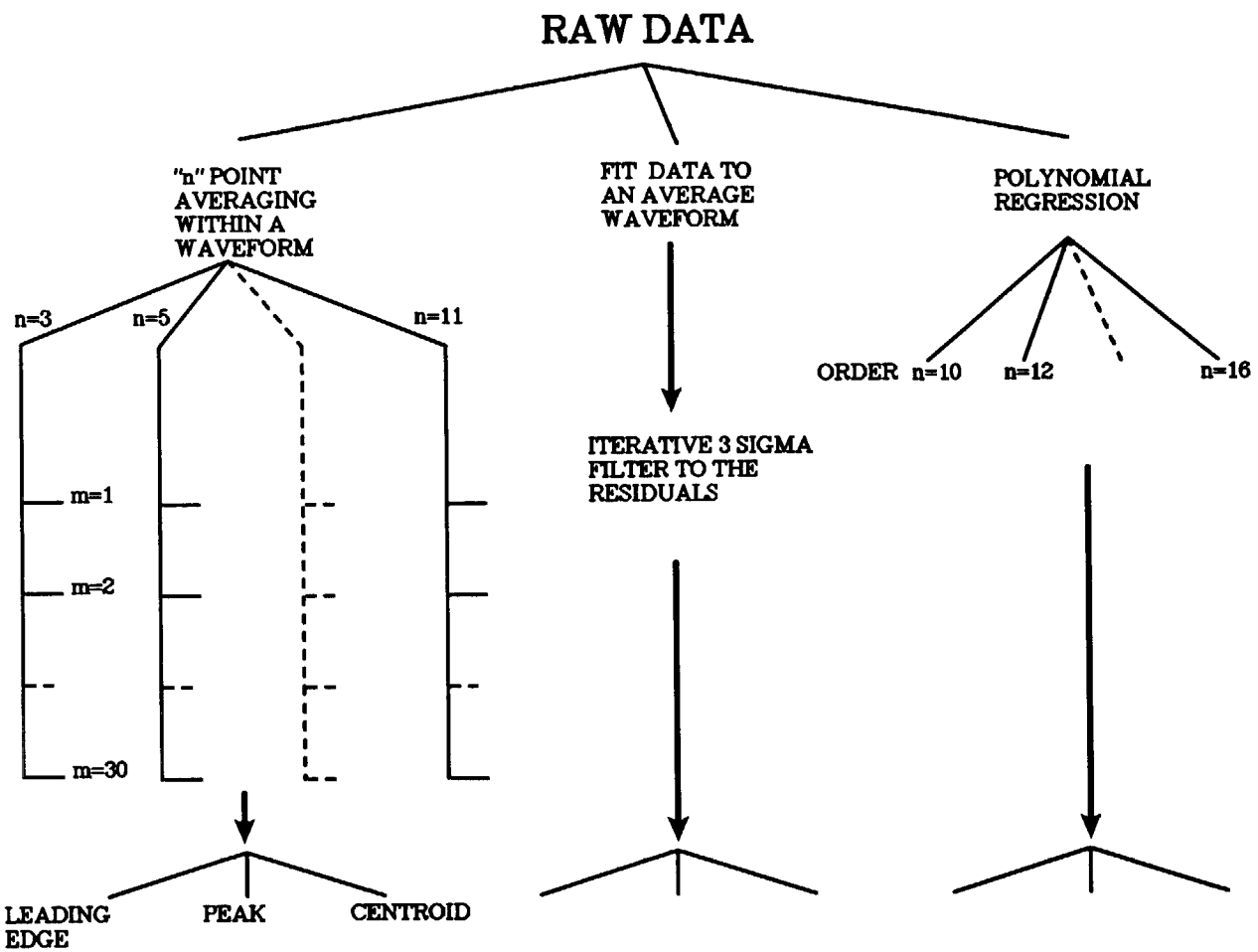

Tree structure illustrating different types of data processing techniques investigated for determination of pulse pair separation. The best results were obtained for data smoothing with n=3 and n=5 while using centroid/leading edge analysis.

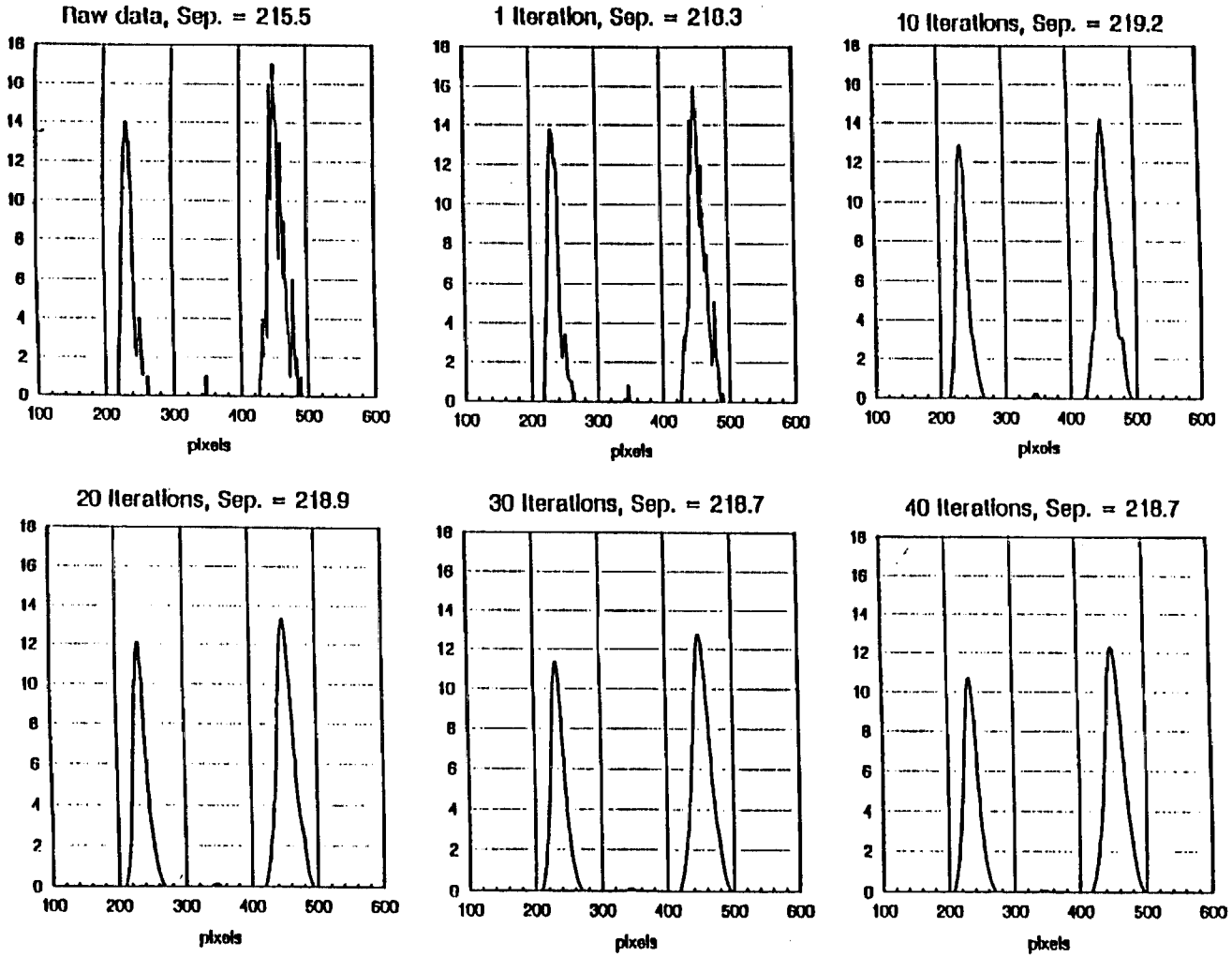

ILLUSTRATION OF THE EVOLUTION OF THE NOISY PULSE PROFILE AS A FUNCTION OF NUMBER OF ITERATIONS OF SMOOTHING (3–POINT). THE PULSE SEPARATION IS STABLE AFTER ABOUT 20 ITERATIONS.

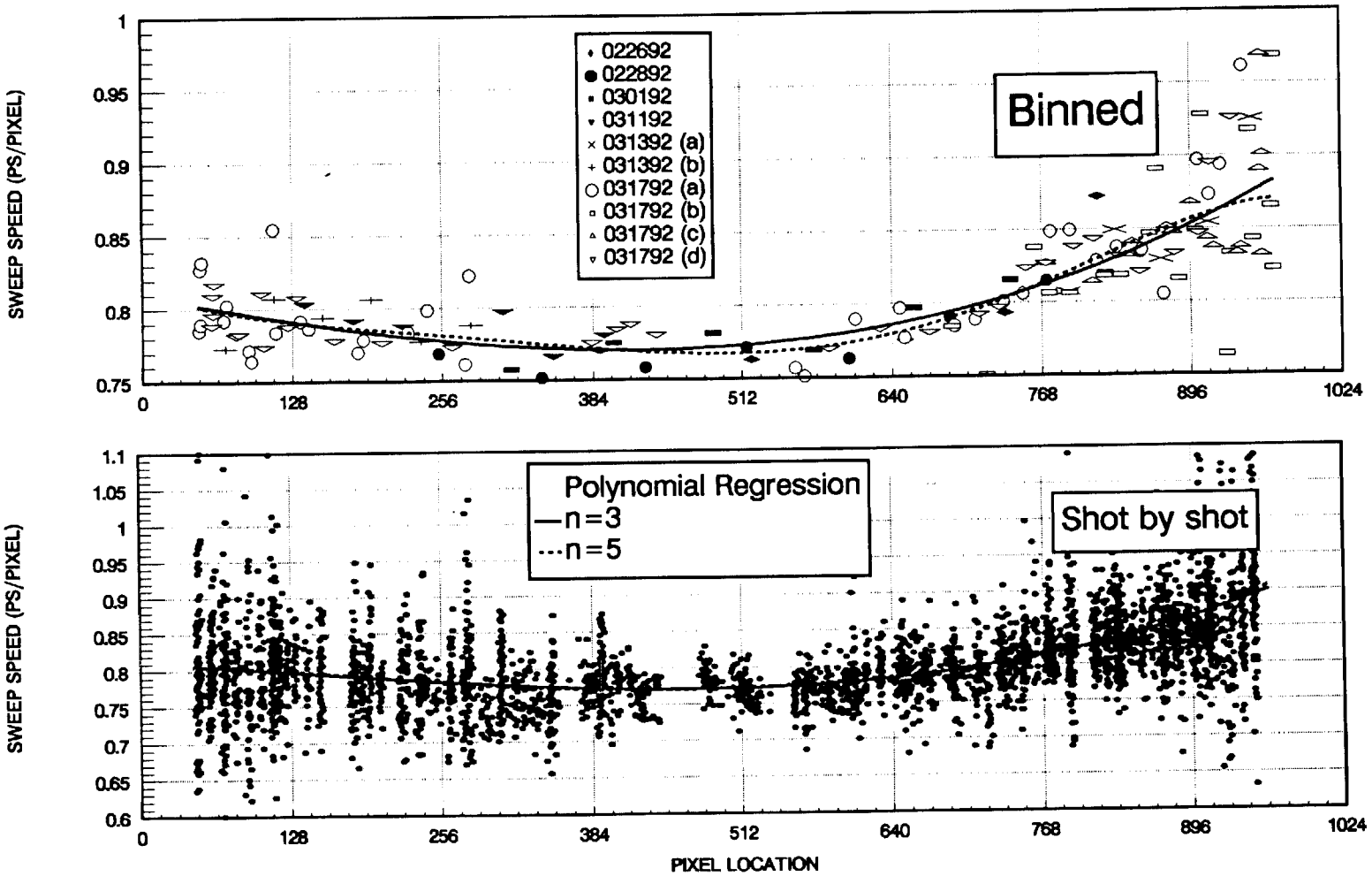

ANALYSIS OF THE NONLINEARITY OF THE SWEEP AS A FUNCTION OF SPATIAL LOCATION. THE TOP PLOT SHOWS NORMAL POINT ANALYSIS FOR A POLYNOMIAL REGRESSION OF N=3 AND N=5 WHILE THE BOTTOM PLOT SHOWS FULL RATE (SINGLE SHOT) ANALYSIS.

SUMMARY

- Single photoelectron sensitive streak camera SLR receive system has been configured with a resolution approaching 250 fs/pixel for high accuracy atmospheric dispersion measurements.
- It has been verified that the streak camera timing characteristics are profoundly impacted by the sweep voltage. The sweep voltage is intrinsically nonlinear in the leading and trailing edges and must be corrected using optical calibration to achieve picosecond timing accuracy. Centroid and half maxima (mean) analyses were found to be superior to peak detection.
- Real-time calibration has been found to be very effective in monitoring the timing performance and would be very advantageous for critical timing measurements.

THE FIRST SATELLITE LASER ECHOES RECORDED ON THE STREAK CAMERA

K.Hamal, I.Procházka

Faculty of Nuclear Science and Physical Engineering, Czech Technical University
Brehova 7,115 19 Prague 1,Czechoslovakia,
Phone/fax +42 2 848840, telex 121254 fjfi c, E-mail TJEAN@CSEARN.BITNET

G.Kirchner, F.Koidl

Austrian Academy of Sciences,Lustbuenel Observatory
A-8042 Graz, Austria, Phone +43 316 472231

ABSTRACT

The application of the streak camera with the circular sweep for the satellite laser ranging is described. The Modular Streak Camera system employing the circular sweep option was integrated into the conventional Satellite Laser System. The experimental satellite tracking and ranging has been performed. The first satellite laser echo streak camera records are presented.

GENERAL

The laser ranging of the artificial Earth satellites, the Moon and the long ground baselines is an attractive and rapidly developing technique. The laser ranging precision and accuracy is gradually increasing, it reaches one centimeter level at present. The goal for nineties, requested by the data users, is the satellite laser ranging to artificial satellites with millimeter accuracy. The existing pulsed laser ranging systems are using short pulse lasers of 20-200 picoseconds at 532 nanometers as a transmitter, the fast microchannel plate photomultiplier tube along with an appropriate electric discriminator or an avalanche photodiode as a return signal detector reaching a time interval resolution of 30 picoseconds. An electronic time interval unit having a resolution of 20-35 picoseconds is used to determine the interval between the laser pulse transmittion and echo signal detection[1].

The limiting factor for the current systems accuracy improvement from centimeter to millimeter level are the currently used detectors and discriminators, time interval meters and the contribution of the target itself. The main contributors to the systematic error and hence limiting the final accuracy is the atmosphere. The existing atmospheric models based on meteorological data permit to predict the atmospheric optical delay with centimeter accuracy. It is expected, that ranging simultaneously on two wavelength and determining the two wavelength propagation time difference, the existing atmospheric models will be improved to millimeter accuracy. However, to obtain the valuable data for atmospheric model improvement, the two wavelength delay must be measured with picosecond accuracy[2] .

The goals of the implementation of a streak camera into a laser ranging system :
The first : the replacement of the existing detectors and discriminators by the streak camera

with and appropriate readout and data processing system. This will increase the time interval resolution of the radar detection chain several times, the echo pulses distortion by the target geometry may be monitored and compensated. The second : the streak camera will be used for two wavelength laser ranging echo signals detection, the two wavelength range delay may be determined with the picosecond accuracy. The third : along with the detector, the streak camera may be integrated into the time interval unit. The picosecond time resolution and a high overall timing accuracy is expected[1].

THE STREAK CAMERA CONSTRUCTION

Designing the streak camera for satellite laser ranging purpose several key problems have to be solved:
- the energy budget of the ranging chain, closely connected to the photocathode and sweep speed used,
- the camera configuration, the type of deflection, input optics configuration,
- the readout system and the output data processing.

Completing the series of indoor and ground target ranging experiments, we have chosen the S25 photocathode, the circular sweep camera setup and a two dimensional TV readout system with a full frame image processing. The linear sweep tube setup reaches higher limiting temporal resolution. However, the necessity of a trigger signal appearing 10-30 nanoseconds prior to the photons to be detected with a subnanosecond jitter and the angular/temporal relation may cause serious difficulties when ranging to satellites. Using the circular sweep tube setup, the trigger signal requirements are moderate : the trigger signal must appear 10-20 microseconds before the optical signal, the jitter of several microseconds is acceptable. The temporal/angular dependence may be monitored, software modelled and compensated.

The PV-006 streak tube having the S25 photocathode and the microchannel plate image intensifier fiber optically coupled together have been used. The streak tube is equipped with two pairs of deflecting plates acting in the mutually perpendicular direction. Applying the RF signal phase shifted to both deflection plate pairs, the circular sweep may be obtained. The 320 MHz signal, 13 Watts of pulsed RF power is used. The maximal RF power applicable on the deflection system is limited by the internal ionization inside the tube. The diameter of the circle was about 6 mm resulting in 155 psec/mm sweep speed. Due to the imperfect impedance matching of the RF driving circuit to the tube deflection system, the deflection is not perfectly circular. Nevertheless, the complex streak image processing and calibration package is able to compensate for these effects. The temporal resolution of 30-35 psec and the range difference jitter 6 psec have been achieved.

The application of the streak camera for ranging purposes is accomplished by the timing and gating circuitry. The deflection signal is ON for only few microseconds before laser transmittion and again few microseconds before expected arrival of the satellite echo. All the remaining time the camera is working in the static image mode and may be used for guiding / alignment purposes, as well. The 320MHz deflection signal is produced by multiplication of the 5 MHz sine wave output of the station Cs beam frequency standard, which is simultaneously acting as an master oscillator for all the station timing electronics. This way, the precise phase synchronism of the radar electronics and the camera circular deflection is maintained. In fact, the camera may be used as a vernier to the time interval unit, rough time interval is derived from the integer number of periods from Start to Stop event, the fraction of the period may be determined from the phase difference of the Start and Stop events[5].

The microchannel plate intensifier gain is controlled in three steps. During the laser

transmittion, the gain is set to minimum to avoid the blinding of the system by the atmospheric backscattered light. Optionally, the mechanical shutter in front of the input photocathode is used. Most of the time the microchannel plate gain is set to 100, a compromise between the static image mode gain and the background noise contribution. At the expected echo arrival time, the gain is set to maximum of 10,000 for 300 microseconds to achieve maximum detection sensitivity.

To readout the tube screen image we use the Silicon Intensified Target (SIT) tube made by Haimann. The output signal was fed to the Visionetics Frame Grabber card (512x512x8bits) inserted in the IBM PC. To solve the problem of a deflection nonsymetry, the software package[3] allows the full frame image processing and accomplishes the software modelling of the image distortion, the sweep nonlinearity, the gain nonuniformity etc. On the end of the image processing procedure the temporal curve consisting of 1000 channels, 8 bits each is generated. Once the center of the deflection circle is identified, for example using the satellite image in the static mode, the temporal/angular effect[4] may be software compensated.

The compact design of the camera, its rugged construction along with its low mass permitted to install it directly on the moving part of the tracking telescope.

SATELLITE LASER RANGING SYSTEM

The streak camera has been integrated to the Satellite Ranging System of the Lustbuehel Observatory, Graz, Austria. The ranging system consists of a modified Quantel laser, passively mode locked NdYAG with the second harmonic generator, delivering pulses of 10 milliJoules, 35 picoseconds in green. Alternatively the semitrain of 5 - 7 such pulses containing totally 60 milliJoules may be transmitted. The telescope is a Contraves laser tracking type. The laser output is transmitted by a 10 cm diameter Galileo telescope, the 0.5 meter diameter Cassegrain optics is used for both return photons collection and visual guiding. The streak camera replaced an original ISIT camera attached to the telescope and dedicated for faint objects visual tracking. The dielectric mirror is directing 99% of the returned photons on the streak photocathode the remaining photons enter the standard detector package based on a single photon avalanche photodiode. All the rest of the satellite laser ranging hard/software remained unchanged. Thanks to the photodiode single photon response capability, the satellite routine ranging capability has been preserved, although with reduced return rate. The streak camera system timing and gating logic has been added.

The streak tube, the image intensifier and the readout have been kept at the temperature + 5 C what resulted in significant dark noise reduction.

RESULTS

The retroreflectors equipped satellites at the distances of 1,000 to 2,300 kilometers have been ranged. The first satellite laser ranging echoes recorded by a streak camera have been obtained January 18,1991 at 21:37 UT from the AJISAI satellite at the distance 2000 km, see **Figure 1**. In this stage, the semitrain of pulses separated by 8.557 nanoseconds has been transmitted. On the image the time interval of 40 milliseconds covering the laser pulse transmittion to echo detection is integrated. The transmitted laser beam backscattered light image is near the center of the pattern displayed in the static image. At this moment the satellite was not illuminated by the Sun. On **Figure 2** there is a streak camera record of the AJISAI satellite echo obtained transmitting single picosecond pulse containing 10 mJ of energy. The temporal profile of the firs part of the trace is included. Please, note the streak camera receiver system saturation by the strong echo signal coming from the first rows of the

corner reflectors. The satellite is a sphere of diameter exceeding two meters covered with retroreflectors. According to numerical simulations, the returned pulse should be spread over the time interval about one nanosecond depending on the satellite orientation. The separate echoes coming from various retroreflectors may be clearly distinguished. The sweep speed nonlinearity has not been compensated on this display. The central spot is an static image of the satellite illuminated by the Sun, thus marking the center of the sweep. The atmospheric backscattered light has been blocked out by the mechanical shutter. The STARLETTE satellite echo record is on **Figure 3**. Single picosecond pulse has been transmitted. The satellite is a sphere covered with retroreflectors of the diameter of about 25 centimeters at a distance about 1,000 kilometers. The echo signal time spread is significantly smaller in comparison to the AJISAI satellite. The temporal profile of the echo is included, as well. The detector saturation may be seen. The system temporal resolution may be demonstrated on the not saturated response from a single corner reflector resulting in a pulse width of 25-30 picoseconds.

CONCLUSION

The first satellite laser echoes have been recorded on the streak camera to our knowledge for the first time. The applicability of a Modular Streak Camera system employing the circular sweep for satellite laser ranging has been demonstrated. The sensitivity of the streak camera has been confirmed to be satisfactory for the purpose : for standard geodetic satellite ranging employing available laser ranging technology.

REFERENCES

1. J.J.Degnan, "Satellite Laser Ranging: Current Status and Future Prospects", IEEE Trans.on Geoscience and Remote Sensing, Vol. GE-23,pp.398-413,July 1985
2. J.Abshire, Applied Optics, Vol.19, No 20,pp.3436-3440, 1980
3. P.Valach," Streak Camera Full Frame Image Processing", proc.of the Seventh International Workshop on Laser Ranging Instrumentation,Matera, Oct.1989, edited by C.Veilet,CERGA,France
4. I.Prochazka, K.Hamal, "Streak Camera as a Laser Radar Receiver, its Performance and Limitations", proc. of the Sixth International Workshop on Laser Ranging Instrumentation, Antibes, Sept.1986, edited by J.Gaignebet,Cerga,France,1987
5. K.Hamal, I.Prochazka, M.Schelev, V.Lozovoi, V.Postovalov, " Modular Streak Camera for Ranging", presented at the 19th International Congress on High Speed Photography and Photonics, Cambridge, UK,Sept.17-21,1991, published in SPIE 1358-55

SATELLITE LASER RANGING

FIRST STREAK RECORDS

AJISAI satellite , diameter 2. meters
range 1 500 km
January 19, 1991 , UT 21:37

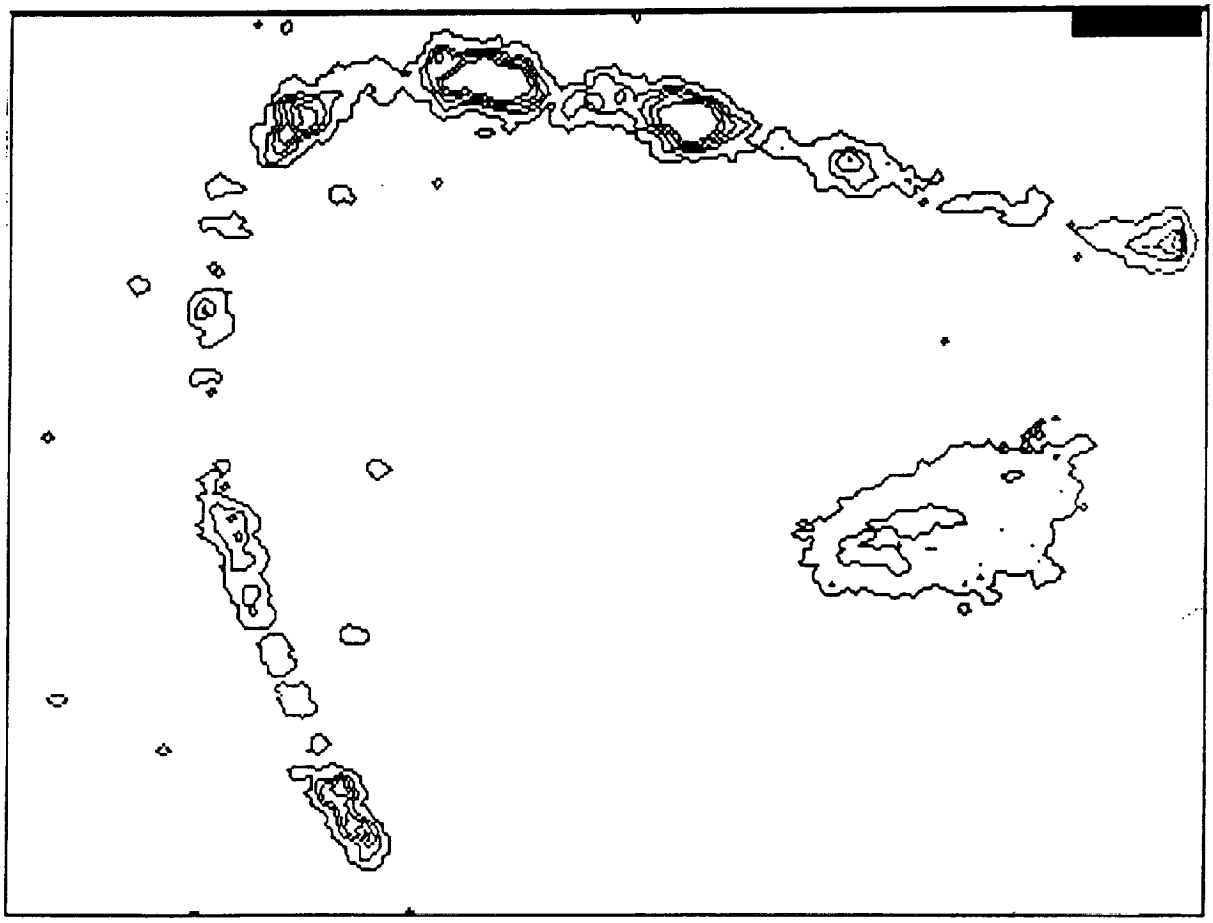

sweep period 3.125 nsec, displayed part 1 nsec

Fig. 1

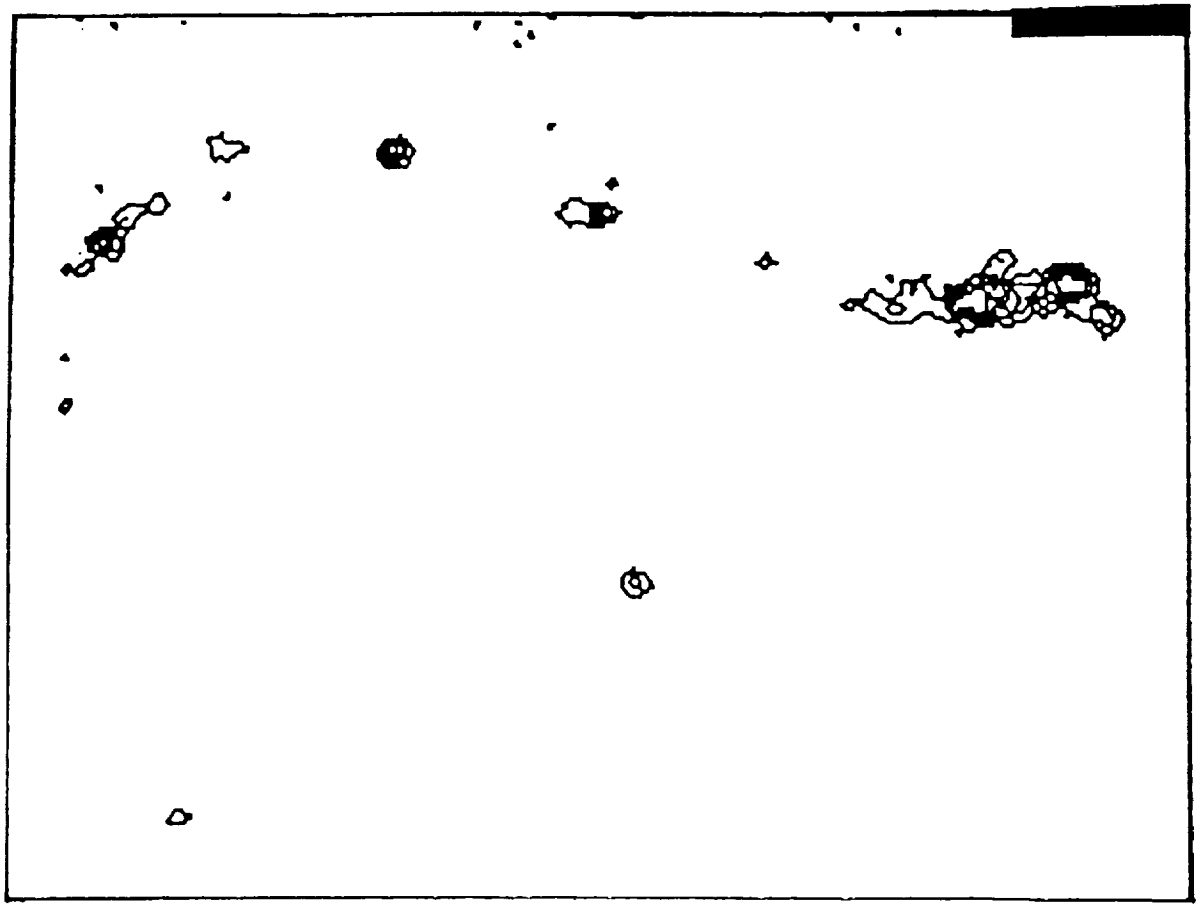

amplitude AJISAI satellite picosecond laser pulse response on streak

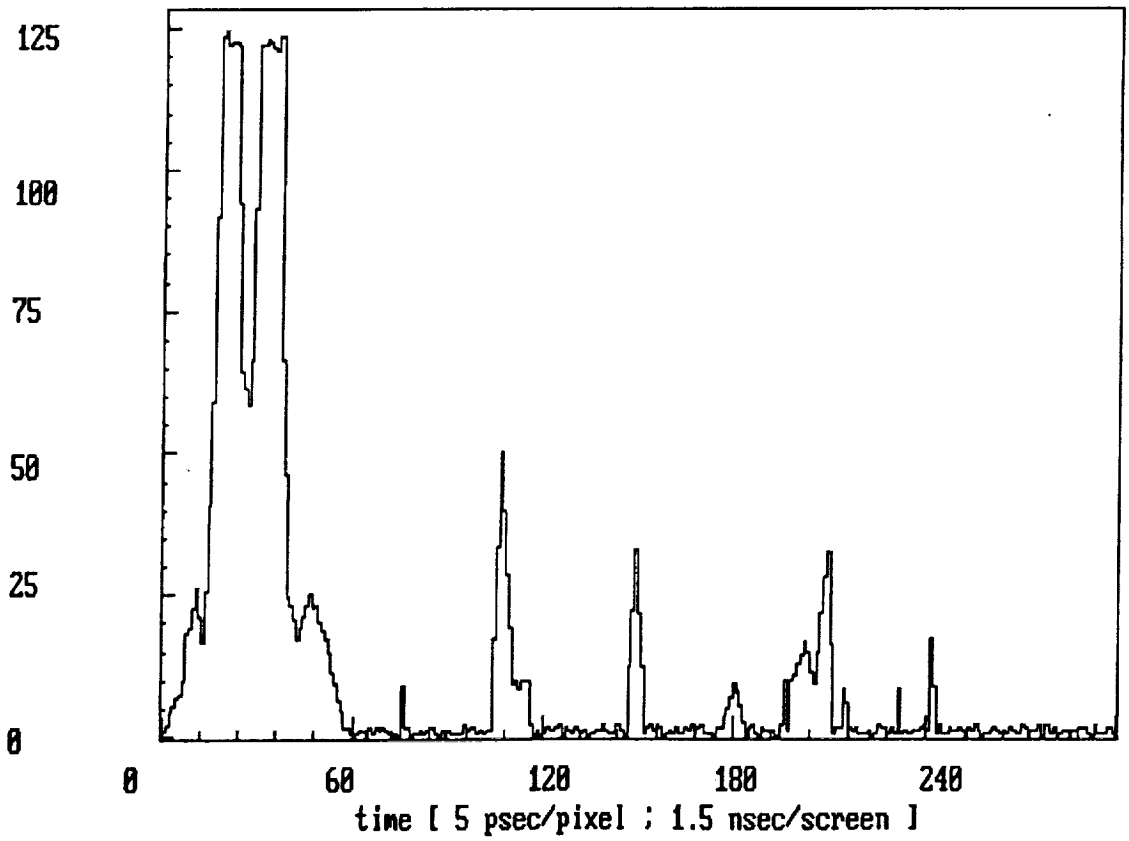

Fig. 2

SATELLITE LASER RANGING

FIRST STREAK RECORDS

STARLETTE satellite , diameter 0.3 meter
range 1 000 km
January 24, 1991 , UT 21:59

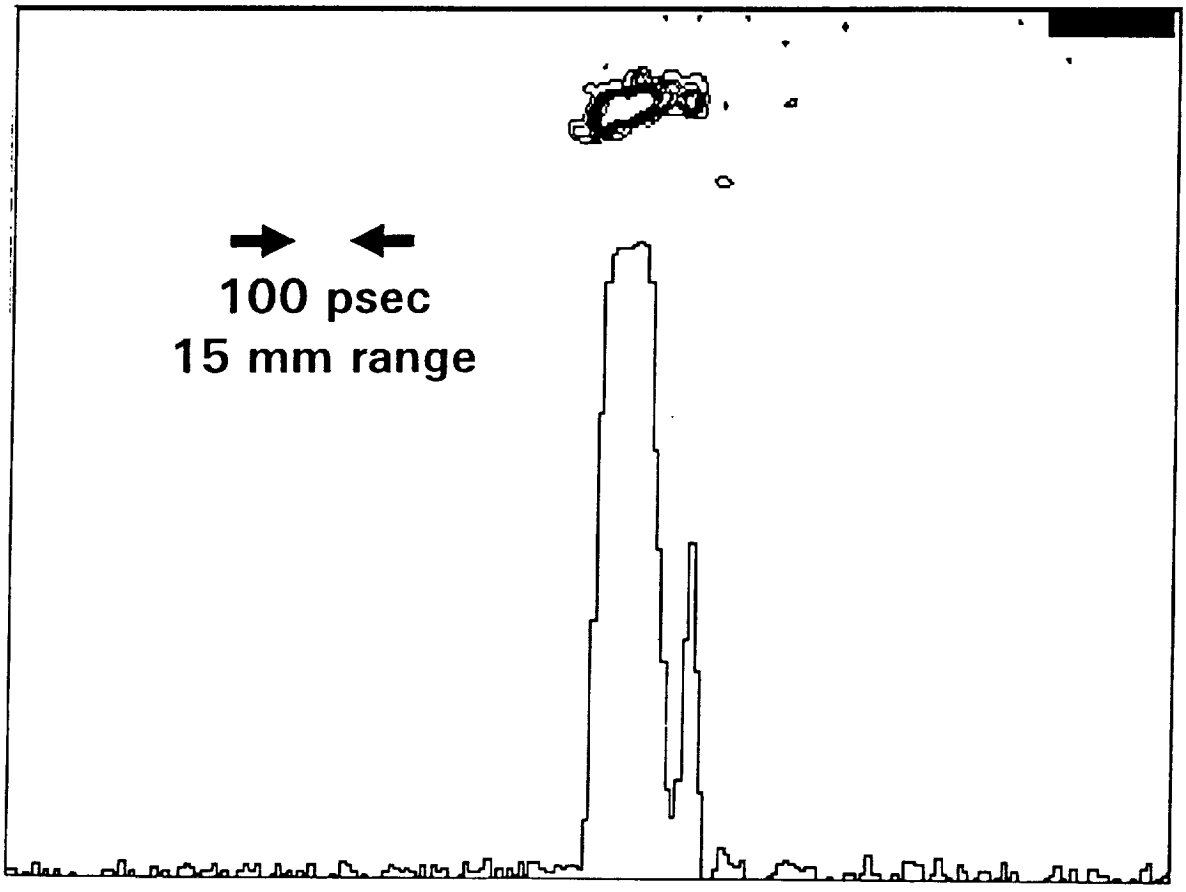

echo signal temporal profile 8 psec / pixel

Fig. 3